Table 1 Clinical findings and MDSCs

Clinical characteristics	MDSC ratio ≥22 ($n = 39$)	MDSC ratio <22 ($n = 84$)	p value
Age (year)	68.5	70.1	0.646
Sex (M/F)	29/10	54/30	0.267
AST (IU/l)	62.0	61.5	0.543
ALT (IU/l)	47.1	53.9	0.759
LDH (IU/l)	225	218	0.832
γGTP (IU/l)	78.0	76.0	0.252
Platelet (10^4/μl)	10.9	10.6	0.884
Prothrombin time (%)	75.2	82.3	0.045
Serum albumin (g/dl)	3.53	3.68	0.120
Total bilirubin (mg/dl)	1.21	0.94	0.286
WBC (/μl)	3910	3610	0.235
Neutrophil (%)	63.2	59.4	0.093
Lymphocyte (%)	26.1	29.5	0.047
Total cholesterol (mg/dl)	151	149	0.926
HbA1c (%)	5.27	5.43	0.197
Type IV collagen 7S (ng/ml)	8.2	7.3	0.086
DCP (mAU/ml)	5157	432	0.561
AFP (ng/ml)	1301	934	0.240
Tumor size (mm)	28.3	24.4	0.014
Tumor multiplicity (multiple/solitary)	27/12	42/42	0.046
TNM stage (I plus II/III plus IV)	17/22	60/24	0.003
Child-Pugh (A/B/C)	20/17/2	64/16/4	0.015
Etiology (HCV/HBV/others)	21/11/7	61/11/12	0.081
$CD4^+$ $CD25^+$ $CD127^{-/low}$ Tregs/ $CD4^+$ cells (%)	7.04	6.70	0.281

AST aspirate aminotransferase, *ALT* alanine aminotransferase, *LDH* lactic dehydrogenase, *γGTP* gamma glutamyltransferase, *WBC* white blood cell, *Hb* hemoglobin, *DCP* des-gamma-prothrombin, *AFP* alpha-fetoprotein, *HCV* hepatitis C virus, *HBV* hepatitis B virus, *Tregs* regulatory T cells

Chi-squared test with Yates' correction, unpaired t test, Mann–Whitney U test, and Kruskal–Wallis test were used for univariate analysis of two groups that were classified according to the frequency of MDSCs

multiplicity ($p = 0.010$) were significantly associated with HCC recurrence (Table 3). In multivariable analysis for recurrence, considering the variables in the univariate analysis with $p < 0.1$, only post-treatment MDSC ratio ≥22 % (HR 3.906, $p = 0.014$) was extracted as a significant risk factor for recurrence.

Discussion

MDSCs are expanded in pathological conditions such as malignancy, infection, or trauma and consist of a heterogeneous population of immature myeloid cells [15, 25]. In pathological conditions, immature myeloid cells are blocked to differentiate into mature macrophages, dendritic cells, or granulocytes; as a result, MDSCs are accumulated [15, 25]. MDSCs strongly inhibit anti-tumor immune response through a number of mechanisms [15, 25]. As monocytic subsets of MDSCs, $CD14^+HLA\text{-}DR^{-/low}$ MDSCs have been reported in various malignancies, including melanoma, multiple myeloma, prostate cancer, and bladder cancer [18, 20, 22, 35]. In the most recent study, Hoechst et al. [24] reported that $CD14^+HLA\text{-}DR^{-/low}$ MDSCs were significantly increased in HCC patients and they suppressed T cell functions through the induction of $CD4^+CD25^+Foxp3^+$ Treg.

In the present study, in addition to an increase in the number of MDSCs in HCC patients, we observed that the frequency was correlated with the progression of HCC. Consistent with our results, it has also been reported that the frequency of $CD14^+HLA\text{-}DR^{-/low}$ MDSCs was correlated with tumor progression in patients with other cancers, such as melanoma, prostate cancer, and bladder cancer [22, 35, 36]. However, the mechanisms behind the increase in MDSCs in advanced cancer patients are still unclear. As is well known, there is a close relationship between hepatocarcinogenesis and histological status of underlying liver [37, 38]. Therefore, the advance of hepatic fibrosis and the increase in inflammatory cell infiltration into liver might result in an increase in MDSCs following the progression of HCC. However, there was no relationship between the frequency of $CD14^+HLA\text{-}DR^{-/low}$ MDSCs and underlying liver status in our study. From our observations, increase in MDSCs was only correlated with tumor progression, but not with hepatic fibrosis or disease activity of CLD. This finding suggests that the expansion of $CD14^+HLA\text{-}DR^{-/low}$ MDSCs was mostly derived from the tumor environment itself, but not from inflammation or fibrosis of liver tissue around the tumor. The finding that a significant decrease in the frequency of circulating $CD14^+HLA\text{-}DR^{-/low}$ MDSCs is observed in most patients with curative treatment in this study supports this hypothesis. On the other hand, Tregs were also increased in HCC patients and associated with the progression of HCC. Though it was reported that MDSCs suppressed T cell function through the induction of Tregs, there was not a strong correlation between the frequencies of these two immunosuppressive cells.

Regarding the mechanism of MDSC expansion, we also analyzed the relationship between the serum cytokine levels and the frequency of MDSCs. We observed that the serum concentrations of IL-10, IL-13, and VEGF were significantly increased in the group with high frequency of MDSCs and there was a positive correlation between these cytokine levels and the frequency of MDSCs. Moreover, although there was no significant difference, the serum

Table 2 Serum cytokines and MDSCs

Cytokine	Healthy donor (mean) ($n = 13$)	MDSC ratio ≥ 22 (mean) ($n = 21$)	Range	MDSC ratio < 22 (mean) ($n = 31$)	Range	p value
IL-1ra	34.2	97.0	(21.5–600)	40.3	(3.4–151)	0.057
IL-2	10.5	38.1	(4.3–54.3)	11.3	(0.9–49.7)	0.055
IL-4	2.6	5.75	(1.47–11.9)	5.03	(0.71–10.9)	0.159
IL-6	9.9	21.5	(1.2–130)	10.1	(0.2–97.2)	0.065
IL-8	24.5	64.7	(10.9–291)	35.1	(6.2–142)	0.156
IL-10	2.76	6.01	(0.8–11.5)	2.81	(0.1–12.0)	0.003
IL-12(p70)	14.6	33.3	(0.6–140)	17.6	(1.4–57)	0.058
IL-13	7.6	13.1	(1.2–33.6)	8.2	(2.7–22.9)	0.015
IL-17	15.7	23.5	(4.6–70)	20.8	(2.1–119)	0.115
Eotaxin	104	141	(51.9–493)	124	(26.3–331)	0.675
G-CSF	7.9	13.2	(2.7–41.3)	8.7	(0.5–17.9)	0.050
IFN-γ	52.6	95.4	(23.1–417)	69.9	(2.5–238)	0.136
MCP-1	20.2	26.8	(8.4–114)	23.8	(3.5–77)	0.744
MIP-1b	97.6	120	(58.3–490)	108	(39.7–263)	0.508
PDGF	4012	4375	(1,312–10,136)	4013	(831–13,557)	0.484
RANTES	2978	2890	(1,040–4,826)	3184	(599–6,165)	0.186
TNF-α	10.5	34.9	(0.1–175)	27.6	(2.9–105)	0.756
VEGF	34.6	101.7	(22.5–371)	59.5	(9.3–183)	0.045

IL interleukin, *G-CSF* granulocytic colony stimulating factor, *IFN* interferon, *MCP* monocyte chemoattractant protein, *MIP* macrophage inflammatory protein, *PDGF* platelet-derived growth factor, *RANTES* regulated upon activation, normal T cell expressed and secreted, *TNF* tumor necrosis factor, *VEGF* vascular endothelial growth factor

Mann–Whitney *U* test was used for univariate analysis of two groups that were classified according to the frequency of MDSCs

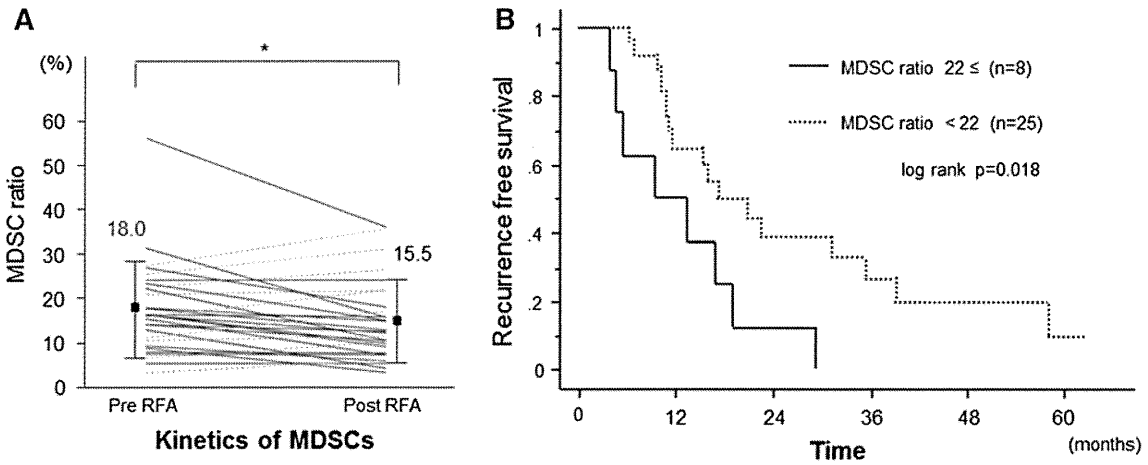

Fig. 3 **a** In 33 HCC patients who received curative RFA therapy, the frequency of MDSCs was significantly decreased after treatment. However, in several patients, the frequencies were increased after treatment (*dotted lines*) (*, $p < 0.05$). **b** Kaplan–Meier curve for recurrence-free survival after RFA therapy. The patients with high frequency of MDSCs (*solid line*) relapsed

concentrations of IL-1ra, IL-2, IL-6, IL-12(p70), and G-CSF tended to be increased in the group with high frequency of MDSCs. In accordance with our results, various cytokines, including IL-6, IL-10, IL-13, G-CSF, and VEGF, that trigger Janus kinase (JAK)-signal transducer and activator of transcription (STAT) signaling pathways have been reported to be associated with the frequency of MDSCs [39]. In particular, the cytokines involved in the JAK2-STAT3 signaling pathway are considered to be the main regulators of the expansion of MDSCs, which leads to stimulation of myelopoiesis and inhibition of myeloid-cell differentiation [40–42].

Table 3 Cox proportional hazards regression for recurrence

Variant	Univariate HR (95 % CI)	*p* value	Multivariable HR (95 % CI)	*p* value
Sex: female	0.763 (0.446–1.308)	0.326		
Age: ≥70 years	1.111 (0.671–1.840)	0.683		
Pre-MDSC ratio: ≥22 %	1.210 (0.698–2.096)	0.497		
Pre-neutrophil	0.990 (0.969–1.012)	0.385		
Pre-lymphocyte	1.014 (0.987–1.043)	0.311		
Pre-neutrophil/lymphocyte	0.978 (0.787–1.216)	0.844		
Pre-ALT	1.001 (0993–1.008)	0.882		
Pre-serum albumin: <3.5 mg/dl	1.143 (0.665–1.982)	0.647		
Pre-prothrombin time: <70 %	1.662 (0.961–2.903)	0.073	1.881 (0.522–6.777)	0.101
Post-MDSC ratio: ≥22 %	2.795 (1.150–6.792)	0.023	3.906 (1.313–11.616)	0.014
Post-neutrophil	1.005 (0.975–1.035)	0.762		
Post-lymphocyte	0.993 (0.960–1.027)	0.678		
Post-neutrophil/lymphocyte	1.003 (0.810–1.242)	0.980		
Post-ALT	0.995 (0.981–1.010)	0.501		
Type IV collagen 7S	1.122 (0.992–1.268)	0.067	1.192 (0.907–1.566)	0.207
AFP: ≥100 ng/ml	1.357 (0.743–2.480)	0.321		
Tumor size: ≥20 mm	1.29 (0.78–2.12)	0.328		
Tumor multiplicity: multiple	2.00 (1.18–3.40)	0.010	1.851 (0.721–4.753)	0.201

HR hazard ratio, *CI* confidence interval, *ALT* alanine aminotransferase, *AFP* alpha-fetoprotein

Another important finding of our study is that the frequency of MDSCs showed various changes after curative RFA and this frequency is an independent risk factor of HCC recurrence. In most of the patients, the frequency of MDSCs decreased after RFA. A similar phenomenon has also been reported in other cancer treatments [19, 21, 36]. Liu et al. [21] reported that MDSCs were decreased in non-small cell lung cancer patients who had clinical benefit from chemotherapy or who received curative surgery. These results suggest that a decrease in the frequency of MDSCs is due to tumor eradication.

It is well known that tumor factors including multiplicity, tumor diameter, serum levels of tumor marker, and hepatic reserve are risk factors of HCC recurrence after RFA [43, 44], but it has not been reported that the frequency of circulating MDSCs is also a risk factor. From our findings, there was a clear inverse correlation between the frequency of MDSCs after RFA and recurrence-free survival. Consistent with our results, in the patients with pancreatic, esophageal, and gastric cancer, Gabitass et al. [23] reported that an increase in MDSCs was associated with an increased risk of death and that the frequency of MDSCs was an independent prognostic factor for patient survival. Taken together with these findings, our results suggest that the frequency of MDSCs might be one of the prognostic factors of patients after cancer treatments.

As we showed, the frequency of MDSCs is primarily correlated with tumor progression. However, between the patients with high and low frequency of MDSCs after RFA, there was no significant difference in hepatic reserve and tumor factors before treatment. Although an incomplete HCC eradication at a microscopic level may allow a high frequency of MDSCs after RFA, there may be other mechanisms such as subsequently tumor-specific immune responses after RFA. In addition, there is a limitation of the present study because we used cryopreserved PBMCs for phenotypic analysis of MDSCs. Further studies using fresh PBMCs are needed for precise phenotypic analysis of MDSCs and elucidation of the mechanism to regulate the frequency of MDSCs after HCC treatment.

In conclusion, the frequency of MDSCs in HCC patients is correlated with tumor progression, and the frequency after RFA is inversely correlated with the prognosis of HCC patients. HCC patients who show a high frequency of MDSCs after RFA should be closely followed, and the inhibition or elimination of MDSCs after HCC treatments may improve the prognosis of HCC patients.

Acknowledgments This study was supported by research grants from the Ministry of Education, Culture, Sports, Science and Technology of Japan.

Conflict of interest The authors declare no conflict of interest.

References

1. Thomas MB, Jaffe D, Choti MM, Belghiti J, Curley S, Fong Y, Gores G (2010) Hepatocellular carcinoma: consensus recommendations of the National Cancer Institute Clinical Trials Planning Meeting. J Clin Oncol 28:3994–4005

2. Llovet JM, Burroughs A, Bruix J (2003) Hepatocellular carcinoma. Lancet 362:1907–1917
3. Lencioni R, Chen XP, Dagher L, Venook AP (2010) Treatment of intermediate/advanced hepatocellular carcinoma in the clinic: how can outcomes be improved? Oncologist 15 Suppl 4:42–52
4. Curley SA, Izzo F, Ellis LM, Nicolas Vauthey J, Vallone P (2000) Radiofrequency ablation of hepatocellular cancer in 110 patients with cirrhosis. Ann Surg 232:381–391
5. Ishizaki Y, Kawasaki S (2008) The evolution of liver transplantation for hepatocellular carcinoma (past, present, and future). J Gastroenterol 43:18–26
6. Yamashita T, Arai K, Sunagozaka H, Ueda T, Terashima T, Mizukoshi E, Sakai A (2011) Randomized, phase II study comparing interferon combined with hepatic arterial infusion of fluorouracil plus cisplatin and fluorouracil alone in patients with advanced hepatocellular carcinoma. Oncology 81:281–290
7. Llovet JM, Ricci S, Mazzaferro V, Hilgard P, Gane E, Blanc JF, de Oliveira AC (2008) Sorafenib in advanced hepatocellular carcinoma. N Engl J Med 359:378–390
8. Butterfield LH (2004) Immunotherapeutic strategies for hepatocellular carcinoma. Gastroenterology 127:S232–S241
9. Sun K, Wang L, Zhang Y (2006) Dendritic cell as therapeutic vaccines against tumors and its role in therapy for hepatocellular carcinoma. Cell Mol Immunol 3:197–203
10. Zerbini A, Pilli M, Penna A, Pelosi G, Schianchi C, Molinari A, Schivazappa S (2006) Radiofrequency thermal ablation of hepatocellular carcinoma liver nodules can activate and enhance tumor-specific T-cell responses. Cancer Res 66:1139–1146
11. Palmer DH, Midgley RS, Mirza N, Torr EE, Ahmed F, Steele JC, Steven NM (2009) A phase II study of adoptive immunotherapy using dendritic cells pulsed with tumor lysate in patients with hepatocellular carcinoma. Hepatology 49:124–132
12. Mizukoshi E, Nakamoto Y, Arai K, Yamashita T, Sakai A, Sakai Y, Kagaya T (2011) Comparative analysis of various tumor-associated antigen-specific t-cell responses in patients with hepatocellular carcinoma. Hepatology 53:1206–1216
13. Whiteside TL (2006) Immune suppression in cancer: effects on immune cells, mechanisms and future therapeutic intervention. Semin Cancer Biol 16:3–15
14. Khattri R, Cox T, Yasayko SA, Ramsdell F (2003) An essential role for Scurfin in CD4 + CD25 + T regulatory cells. Nat Immunol 4:337–342
15. Gabrilovich DI, Nagaraj S (2009) Myeloid-derived suppressor cells as regulators of the immune system. Nat Rev Immunol 9:162–174
16. Zea AH, Rodriguez PC, Atkins MB, Hernandez C, Signoretti S, Zabaleta J, McDermott D (2005) Arginase-producing myeloid suppressor cells in renal cell carcinoma patients: a mechanism of tumor evasion. Cancer Res 65:3044–3048
17. Gordon IO, Freedman RS (2006) Defective antitumor function of monocyte-derived macrophages from epithelial ovarian cancer patients. Clin Cancer Res 12:1515–1524
18. Filipazzi P, Valenti R, Huber V, Pilla L, Canese P, Iero M, Castelli C (2007) Identification of a new subset of myeloid suppressor cells in peripheral blood of melanoma patients with modulation by a granulocyte-macrophage colony-stimulation factor-based antitumor vaccine. J Clin Oncol 25:2546–2553
19. Diaz-Montero CM, Salem ML, Nishimura MI, Garrett-Mayer E, Cole DJ, Montero AJ (2009) Increased circulating myeloid-derived suppressor cells correlate with clinical cancer stage, metastatic tumor burden, and doxorubicin-cyclophosphamide chemotherapy. Cancer Immunol Immunother 58:49–59
20. Brimnes MK, Vangsted AJ, Knudsen LM, Gimsing P, Gang AO, Johnsen HE, Svane IM (2010) Increased level of both CD4 + FOXP3 + regulatory T cells and CD14 + HLA-DR$^-$/low myeloid-derived suppressor cells and decreased level of dendritic cells in patients with multiple myeloma. Scand J Immunol 72:540–547
21. Liu CY, Wang YM, Wang CL, Feng PH, Ko HW, Liu YH, Wu YC (2010) Population alterations of L-arginase- and inducible nitric oxide synthase-expressed CD11b +/CD14$^-$/CD15 +/CD33 + myeloid-derived suppressor cells and CD8 + T lymphocytes in patients with advanced-stage non-small cell lung cancer. J Cancer Res Clin Oncol 136:35–45
22. Vuk-Pavlović S, Bulur PA, Lin Y, Qin R, Szumlanski CL, Zhao X, Dietz AB (2010) Immunosuppressive CD14 + HLA-DRlow/- monocytes in prostate cancer. Prostate 70:443–455
23. Gabitass RF, Annels NE, Stocken DD, Pandha HA, Middleton GW (2011) Elevated myeloid-derived suppressor cells in pancreatic, esophageal and gastric cancer are an independent prognostic factor and are associated with significant elevation of the Th2 cytokine interleukin-13. Cancer Immunol Immunother 60:1419–1430
24. Hoechst B, Ormandy LA, Ballmaier M, Lehner F, Krüger C, Manns MP, Greten TF (2008) A new population of myeloid-derived suppressor cells in hepatocellular carcinoma patients induces CD4(+)CD25(+)Foxp3(+) T cells. Gastroenterology 135:234–243
25. Ostrand-Rosenberg S, Sinha P (2009) Myeloid-derived suppressor cells: linking inflammation and cancer. J Immunol 182:4499–4506
26. Youn JI, Nagaraj S, Collazo M, Gabrilovich DI (2008) Subsets of myeloid-derived suppressor cells in tumor-bearing mice. J Immunol 181:5791–5802
27. Greten TF, Manns MP, Korangy F (2011) Myeloid derived suppressor cells in human diseases. Int Immunopharmacol 11:802–807
28. Filipazzi P, Huber V, Rivoltini L (2011) Phenotype, function and clinical implications of myeloid-derived suppressor cells in cancer patients. Cancer Immunol Immunother 61(2):255–263
29. Ormandy LA, Hillemann T, Wedemeyer H, Manns MP, Greten TF, Korangy F (2005) Increased populations of regulatory T cells in peripheral blood of patients with hepatocellular carcinoma. Cancer Res 65:2457–2464
30. Fu J, Xu D, Liu Z, Shi M, Zhao P, Fu B, Zhang Z (2007) Increased regulatory T cells correlate with CD8 T-cell impairment and poor survival in hepatocellular carcinoma patients. Gastroenterology 132:2328–2339
31. Kusmartsev S, Gabrilovich DI (2006) Effect of tumor-derived cytokines and growth factors on differentiation and immune suppressive features of myeloid cells in cancer. Cancer Metastasis Rev 25:323–331
32. Bunt SK, Sinha P, Clements VK, Leips J, Ostrand-Rosenberg S (2006) Inflammation induces myeloid-derived suppressor cells that facilitate tumor progression. J Immunol 176:284–290
33. Bunt SK, Yang L, Sinha P, Clements VK, Leips J, Ostrand-Rosenberg S (2007) Reduced inflammation in the tumor microenvironment delays the accumulation of myeloid-derived suppressor cells and limits tumor progression. Cancer Res 67:10019–10026
34. Lechner MG, Liebertz DJ, Epstein AL (2010) Characterization of cytokine-induced myeloid-derived suppressor cells from normal human peripheral blood mononuclear cells. J Immunol 185:2273–2284
35. Yuan XK, Zhao XK, Xia YC, Zhu X, Xiao P (2011) Increased circulating immunosuppressive CD14(+)HLA-DR(-/low) cells correlate with clinical cancer stage and pathological grade in patients with bladder carcinoma. J Int Med Res 39:1381–1391
36. Poschke I, Mougiakakos D, Hansson J, Masucci GV, Kiessling R (2010) Immature immunosuppressive CD14 + HLA-DR-/low cells in melanoma patients are Stat3hi and overexpress CD80, CD83, and DC-sign. Cancer Res 70:4335–4345

37. Fattovich G, Stroffolini T, Zagni I, Donato F (2004) Hepatocellular carcinoma in cirrhosis: incidence and risk factors. Gastroenterology 127:S35–S50
38. El-Serag HB, Rudolph KL (2007) Hepatocellular carcinoma: epidemiology and molecular carcinogenesis. Gastroenterology 132:2557–2576
39. Bromberg J (2002) Stat proteins and oncogenesis. J Clin Invest 109:1139–1142
40. Nefedova Y, Huang M, Kusmartsev S, Bhattacharya R, Cheng P, Salup R, Jove R (2004) Hyperactivation of STAT3 is involved in abnormal differentiation of dendritic cells in cancer. J Immunol 172:464–474
41. Yu H, Kortylewski M, Pardoll D (2007) Crosstalk between cancer and immune cells: role of STAT3 in the tumour microenvironment. Nat Rev Immunol 7:41–51
42. Cheng P, Corzo CA, Luetteke N, Yu B, Nagaraj S, Bui MM, Ortiz M (2008) Inhibition of dendritic cell differentiation and accumulation of myeloid-derived suppressor cells in cancer is regulated by S100A9 protein. J Exp Med 205:2235–2249
43. Izumi N, Asahina Y, Noguchi O, Uchihara M, Kanazawa N, Itakura J, Himeno Y (2001) Risk factors for distant recurrence of hepatocellular carcinoma in the liver after complete coagulation by microwave or radiofrequency ablation. Cancer 91:949–956
44. Komorizono Y, Oketani M, Sako K, Yamasaki N, Shibatou T, Maeda M, Kohara K (2003) Risk factors for local recurrence of small hepatocellular carcinoma tumors after a single session, single application of percutaneous radiofrequency ablation. Cancer 97:1253–1262

Histidine Augments the Suppression of Hepatic Glucose Production by Central Insulin Action

Kumi Kimura,[1] Yusuke Nakamura,[1] Yuka Inaba,[1] Michihiro Matsumoto,[2] Yoshiaki Kido,[3,4] Shun-ichiro Asahara,[3] Tomokazu Matsuda,[3] Hiroshi Watanabe,[5] Akifumi Maeda,[5] Fuyuhiko Inagaki,[6] Chisato Mukai,[6] Kiyoshi Takeda,[7] Shizuo Akira,[8] Tsuguhito Ota,[9] Hajime Nakabayashi,[10] Shuichi Kaneko,[11] Masato Kasuga,[12] and Hiroshi Inoue[1]

Glucose intolerance in type 2 diabetes is related to enhanced hepatic glucose production (HGP) due to the increased expression of hepatic gluconeogenic enzymes. Previously, we revealed that hepatic STAT3 decreases the expression of hepatic gluconeogenic enzymes and suppresses HGP. Here, we show that increased plasma histidine results in hepatic STAT3 activation. Intravenous and intracerebroventricular (ICV) administration of histidine-activated hepatic STAT3 reduced G6Pase protein and mRNA levels and augmented HGP suppression by insulin. This suppression of hepatic gluconeogenesis by histidine was abolished by hepatic STAT3 deficiency or hepatic Kupffer cell depletion. Inhibition of HGP by histidine was also blocked by ICV administration of a histamine H_1 receptor antagonist. Therefore, histidine activates hepatic STAT3 and suppresses HGP via central histamine action. Hepatic STAT3 phosphorylation after histidine ICV administration was attenuated in histamine H_1 receptor knockout (Hrh1KO) mice but not in neuron-specific insulin receptor knockout (NIRKO) mice. Conversely, hepatic STAT3 phosphorylation after insulin ICV administration was attenuated in NIRKO but not in Hrh1KO mice. These findings suggest that central histidine action is independent of central insulin action, while both have additive effects on HGP suppression. Our results indicate that central histidine/histamine-mediated suppression of HGP is a potential target for the treatment of type 2 diabetes. ***Diabetes* 62:2266–2277, 2013**

From the [1]Department of Physiology and Metabolism, Brain/Liver Interface Medicine Research Center, Kanazawa University, Kanazawa, Japan; the [2]Department of Molecular Metabolic Regulation, Diabetes Research Center, Research Institute, National Center for Global Health and Medicine, Tokyo, Japan; the [3]Division of Diabetes and Endocrinology, Kobe University Graduate School of Medicine, Kobe, Japan; the [4]Division of Analytical Biomedical Sciences, Kobe University Graduate School of Health Sciences, Kobe, Japan; [5]BRAND'S Brain Research Centre, Cerebos Pacific Limited, Singapore, Singapore; the [6]Division of Pharmaceutical Sciences, Graduate School of Medical Sciences, Kanazawa University, Kanazawa, Japan; the [7]Laboratory of Immune Regulation, Department of Microbiology and Immunology, Graduate School of Medicine, Osaka University, Suita, Japan; the [8]Laboratory of Host Defense, Immunology Frontier Research Center, Department of Host Defense, Research Institute for Microbial Diseases, Osaka University, Suita, Japan; the [9]Department of Cell Metabolism and Nutrition, Brain/Liver Interface Medicine Research Center, Kanazawa University, Kanazawa, Japan; the [10]Health Science Service Center, Kanazawa University, Kanazawa, Japan; the [11]Department of Disease Control and Homeostasis, Graduate School of Medical Sciences, Kanazawa University, Kanazawa, Japan; and the [12]Diabetes Research Center, Research Institute, National Center for Global Health and Medicine, Tokyo, Japan.

Corresponding author: Hiroshi Inoue, inoue-h@staff.kanazawa-u.ac.jp.

Received 7 December 2012 and accepted 4 March 2013.

DOI: 10.2337/db12-1701

This article contains Supplementary Data online at http://diabetes.diabetesjournals.org/lookup/suppl/doi:10.2337/db12-1701/-/DC1.

Increased glucose production in type 2 diabetes is caused by elevated gluconeogenesis in the liver (1), while in actual clinical settings, treatment for diabetes includes remedies, such as metformin, that suppress hepatic gluconeogenesis (2). Hepatic gluconeogenesis is controlled by regulating the gene expression of gluconeogenic enzymes, such as phosphoenolpyruvate carboxykinase (PEPCK) and glucose-6-phosphatase (G6Pase) (2). In fact, gene expression of hepatic gluconeogenic enzymes is upregulated in obese animal models of diabetes, including *db/db* mice lacking leptin receptors (3,4), while suppression of gluconeogenic gene expression improves glucose tolerance in *db/db* mice (4–6).

Hormonal and nutrient changes regulate the expression of hepatic gluconeogenic genes by a central-mediated mechanism in addition to direct hepatic action (7,8). Insulin, the most important regulatory factor in gluconeogenesis, suppresses hepatic gluconeogenic gene expression via a central indirect mechanism through brain insulin receptors and via direct action on hepatic insulin receptors (9,10). In rodent studies, the intracerebroventricular (ICV) administration of insulin downregulates gluconeogenic gene expression in the liver and suppresses hepatic glucose production (HGP) (10,11). Conversely, HGP is increased in hypothalamic insulin receptor knockdown rats and neuron-specific insulin receptor knockout (NIRKO) mice (9,10). In addition, inhibition of phosphatidylinositol 3-kinase (PI3-K) in the insulin-signaling pathway in the hypothalamus inhibits the central insulin-dependent suppression of HGP (10). Previously, we revealed the importance of signal transducer and activator of transcription-3 (STAT3) in the central insulin-mediated suppression of gluconeogenesis in the liver. In fact, STAT3 is activated through phosphorylation, which is induced by glucose load in an insulin-dependent manner and also by the ICV administration of insulin (9). Further, liver-specific STAT3-deficient (LST3KO) mice exhibit a defect in the central insulin-mediated suppression of HGP (9), suggesting that hepatic STAT3 plays an important role in this process (9). We also revealed that the upregulation of liver-specific interleukin-6 (IL-6) expression is required for the activation of hepatic STAT3 by central insulin (9).

Changes in nutrients are known to affect hepatic gluconeogenesis via central action similarly to insulin (7,8). Glucose and long-chain fatty acids are known to suppress glucose production in the liver after ICV injection (12,13). Recent studies have reported that plasma amino acid levels are also closely associated with glucose metabolism. In fact, in individuals without diabetes and those with new-onset type 2 diabetes, fasting and 2-h blood glucose levels

after glucose loading correlate positively with the blood concentration of branched-chain amino acids alanine, phenylalanine, and tyrosine and negatively with the concentration of histidine and glutamine (14). However, the function of these amino acids in the central-mediated regulation of gluconeogenesis remains to be fully elucidated, while the branched-chain amino acid leucine reportedly suppresses HGP when administered to the hypothalamus (15). In the current study, we found that plasma histidine acts as a nutrient that suppresses hepatic gluconeogenesis via central-mediated hepatic STAT3 activation.

RESEARCH DESIGN AND METHODS

Experiments using mice were conducted in accordance with the guidelines for the care and use of laboratory animals of Kanazawa University. Male mice (8–10 weeks old) were housed under a 12-h light-dark cycle with free access to food and water. Wild-type C57BL/6J Slc mice were purchased from Japan SLC (Shizuoka, Japan), and histamine H_1 receptor knockout (Hrh1KO) (16) mice were from Oriental Bio Service (Kyoto, Japan). We generated LST3KO mice by crossing albumin-cre and floxed-STAT3 mice (5), while NIRKO mice were generated by crossing Nestin-cre and floxed–insulin receptor mice (17). Floxed-STAT3 and floxed–insulin receptor mice were used as the corresponding controls.

Administration of protein extracts and amino acids. Chicken meat extract was prepared as a protein source for gavage administration. Shredded chicken meat was cooked in a pressure cooker for 270 min and strained, the lipids were removed by centrifugation, and the protein concentration was adjusted. Snakehead fish meat was processed in the same way and used as a low-histidine (Low-His) protein source that did not increase blood histidine levels. After 16 h of fasting, the mice were orally administered protein at 2 g/kg body wt via a feeding tube. Histidine or each amino acid was administered at 0.5 mmol/kg body wt i.p. or intravenously at the concentrations shown in Figs. 2*A* and 5*G* after a 16-h fast.

Tolerance tests and biochemical and endocrine testing. A glucose, pyruvate, or fructose tolerance test was performed after a 16-h fast. For the glucose tolerance test, histidine was injected intraperitoneally at 5 min before injection of 2 g/kg body wt glucose (Otsuka Pharmaceutical, Tokushima, Japan). For the pyruvate or fructose tolerance test, histidine was injected twice at 120 and 5 min before 1 g/kg body wt sodium pyruvate or fructose, respectively (Sigma-Aldrich, St. Louis, MO). Blood glucose levels were measured using a GLUCOCARD G+ Meter (Arkray, Kyoto, Japan). Blood insulin and IL-6 levels were measured using a Mouse Insulin ELISA kit (Shibayagi, Gunma, Japan) or a Quantikine Mouse IL-6 ELISA kit (R&D Systems, Minneapolis, MN). Plasma levels of amino acids were quantified using high-performance liquid chromatography. Hypothalamic histamine levels were measured using a Histamine EIA kit (Bertin Pharma, York, U.K.). Hepatic glycogen levels were measured by the anthrone–sulfuric acid method.

Euglycemic clamp technique. Hyperinsulinemic-euglycemic clamping was performed by injecting the awake and unrestrained mice with human insulin (Eli Lilly, Indianapolis, IN) after a 16-h fast. Blood glucose levels were measured every 10 min and maintained between 90 and 120 mg/dL after intravenous insulin injections were started. Further, between 90 and 120 min after starting insulin administration, we stabilized blood glucose volatility with 20 mg/dL insulin (Supplementary Table 1). We measured the glucose infusion rate (GIR) and plasma [^{3}H]glucose specific activity every 10 min. The R_d under steady-state conditions for plasma glucose concentration was determined from the rate of [^{3}H]glucose infusion divided by the plasma [^{3}H]glucose specific activity. The rate of HGP was obtained from the difference between R_d and GIR. An internal cannula (Plastics One, Roanoke, VA) was inserted into the lateral ventricle, followed by intravenous cannulation 7–10 days later. After 4–6 days of recovery and habituation, a hyperinsulinemic-euglycemic clamp or pancreatic clamp was performed with ICV administration. After a 16-h fast, the mice received an ICV administration of human insulin, histidine, or pyrilamine with an intravenous injection of human insulin and somatostatin, as shown in Fig. 7*A*. Blood glucose levels were maintained between 90 and 120 mg/dL. The mice received 10 nmol/mouse LY294002 (Calbiochem, San Diego, CA), 50 μg/mouse pyrilamine (Wako, Osaka, Japan), 50 nmol/mouse thioperamide (Sigma), pyridylethylamine (TOCRIS Bioscience, Ellisville, MO), or artificial cerebrospinal fluid via the lateral ventricle. For the hyperinsulinemic-euglycemic clamp, pyrilamine was administered to the lateral ventricle (Fig. 5G).

IL-6 neutralizing antibody and Kupffer cell depletion. An IL-6 neutralizing antibody and control IgG (R&D Systems) were injected as previously described (9). Clodronate (LKT Laboratories, St. Paul, MN) was encapsulated into empty liposomes (NOF, Tokyo, Japan), and clodronate-containing liposomes (CLDs) were injected into the mice via the tail vein for two consecutive days to deplete Kupffer cells in the liver. The control mice received empty liposomes. Immunostaining with an anti-Mac-2 antibody (Cedarlane Laboratories, Burlington, Ontario, Canada) was performed to visualize the Kupffer cells.

Western blotting and quantitative PCR. Mouse hepatocytes were isolated as previously described (6). Immunoblotting was performed using anti–phosphorylated (phospho)-STAT3 (Tyr705), anti–phospho-Akt (Thr308), anti–phospho-p70 S6 kinase (Thr389), anti–p70 S6 kinase, anti–phospho-S6 ribosomal protein (Ser235/236), and anti-S6 ribosomal protein antibodies from Cell Signaling Technology (Danvers, MA); anti-STAT3, anti-Akt, anti–G6Pase-α, anti-PEPCK, and anti–insulin receptor β antibodies from Santa Cruz Biotechnology (Santa Cruz, CA); and an anti–β-actin antibody from Sigma. Immunoblot images were representative of at least three independent immunoblot analyses and quantified by densitometry on an LAS-3000 Imager (Fujifilm, Tokyo, Japan).

The results of quantitative PCR were analyzed using the *36B4* gene as an internal control. The primer sequences used in this study are available upon request.

Statistical analysis. Statistical analysis was performed using Student *t* test and one- or two-way ANOVA followed by post hoc tests, and differences were considered significant for P values <0.05.

RESULTS

Improvement of glucose tolerance after histidine administration. Phosphorylation of hepatic Akt and STAT3 was increased at 120 min after the oral administration of the protein extract (Fig. 1*A*). As in our previous study (9), glucose loading activated hepatic Akt and STAT3, suggesting that both the hepatic and central actions of insulin were induced by glucose loading. In addition, protein administration also augmented the activation of these molecules by glucose loading (Fig. 1*A*). The intake of proteins is known to facilitate the secretion of insulin (18); in fact, the continuous administration of somatostatin, which suppresses the secretion of endogenous insulin, kept Akt phosphorylation at a virtually undetectable level after ingestion of the protein extract (Fig. 1*B*), whereas protein intake increased STAT3 phosphorylation even in the presence of somatostatin (Fig. 1*B*). These findings suggest that hepatic STAT3 activation associated with protein intake is independent of the secretion of endogenous insulin. Because blood amino acid levels are increased after the oral administration of proteins (19), we administered individual amino acids intraperitoneally to investigate the effects of blood amino acid levels on hepatic STAT3 activation. We found that the hepatic STAT3 phosphorylation was increased by the administration of histidine and histidine-related amino acids and dipeptides, such as 1-methyl-histidine, β-alanyl-histidine (carnosine), and β-alanyl-1-methyl-histidine (anserine) (Fig. 1*C*). Therefore, we investigated the importance of histidine and histidine-containing dipeptides in the activation of hepatic STAT3 using a protein and Low-His protein extract. Coincident with the plasma concentration of histidine and other histidine-containing dipeptides (Supplementary Table 2), a milder increase in STAT3 phosphorylation was observed in the Low-His group compared with the protein group (Fig. 1*D*).

Because histidine administration activates hepatic STAT3, we then conducted a glucose tolerance test to investigate the role of histidine in glucose homeostasis. With the intraperitoneal administration of 500 μmol/kg body wt histidine, which maintained the blood concentration of histidine close to that obtained after the oral administration of 2 g/kg body wt protein (Supplementary Table 3), blood glucose levels were significantly decreased at 120 min after glucose loading (Fig. 1*E*). Conversely, there was no change in plasma insulin levels after histidine administration (Fig. 1*F*). Phosphorylation of hepatic STAT3 increased at 120 min after histidine administration, which was further increased

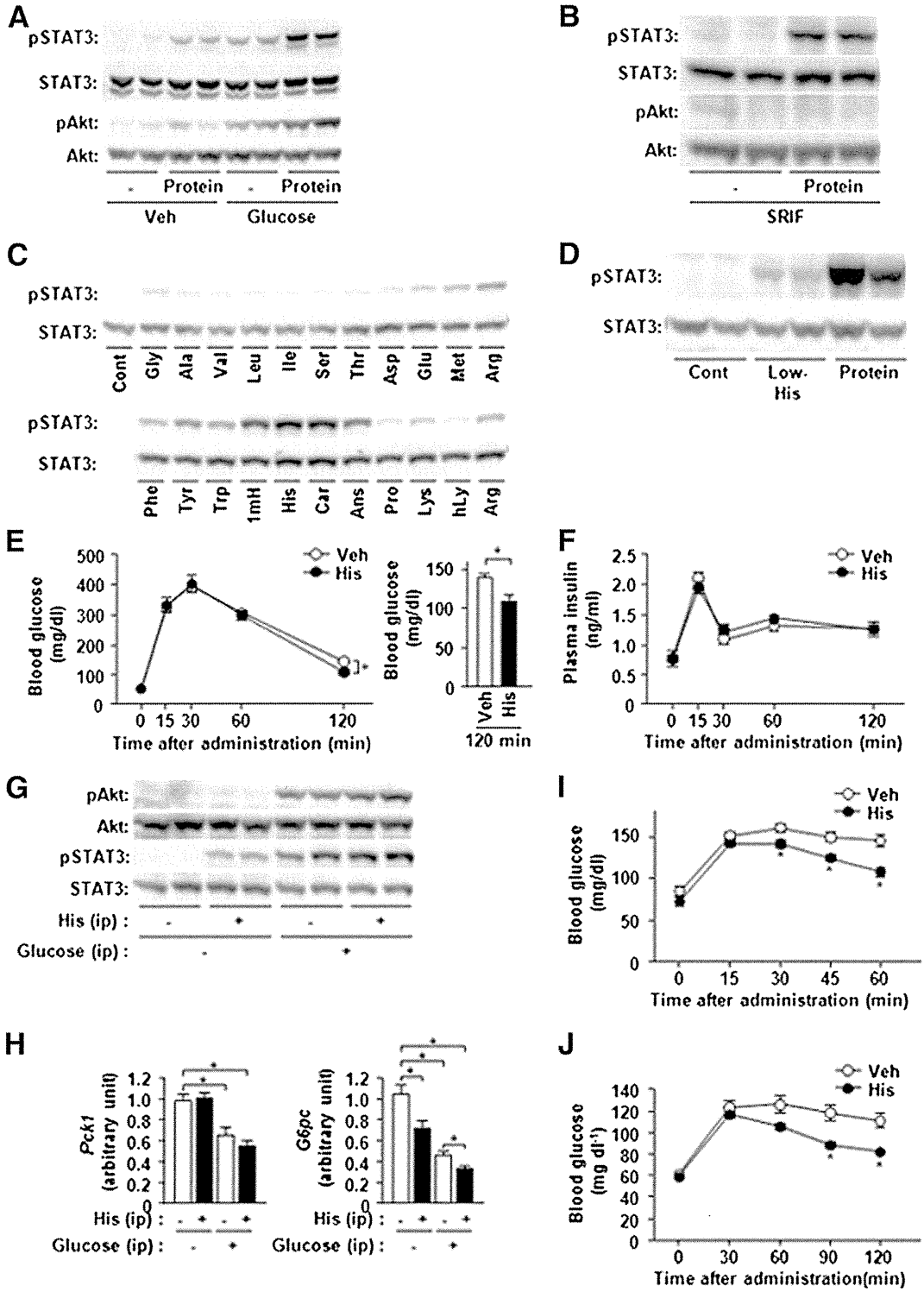

FIG. 1. Phosphorylation of hepatic STAT3 after protein or histidine administration. *A*: Western blotting was performed to analyze the phosphorylation of STAT3 and Akt in the liver at 120 min after the oral administration of protein extract (2 g/kg body wt) and injection of glucose (2 g/kg body wt i.p.) or saline. *B*: Somatostatin was injected continuously at 3 $\mu g \cdot kg^{-1} \cdot min^{-1}$ via the jugular vein, and phosphorylation of hepatic STAT3 and Akt was analyzed at 120 min after the oral administration of protein. *C*: Phosphorylation of hepatic STAT3 was analyzed by Western blotting at 120 min after the intraperitoneal administration of amino acids (0.5 mmol/kg). The experiment was performed in quadruplicate ($n = 4$), and samples were combined for Western blot analysis. 1 mH, 1-methyl-histidine; Ans, anserine; Car, carnosine; and hLy, hydroxylysine. *D*: Phosphorylation of STAT3 was analyzed at 120 min after the oral administration of protein or Low-His. *E* and *F*: A glucose tolerance test was performed with the intraperitoneal administration of histidine (His) or saline (Veh). Changes in blood glucose levels (*E*) (*left panel*), blood glucose levels at 120 min after glucose loading (*E*) (*right panel*), and changes in plasma insulin levels (*F*) are shown. $^*P < 0.05$ ($n = 10$). *G* and *H*: Western blotting analysis of hepatic STAT3 and Akt phosphorylation (*G*) and quantitative PCR analysis of *Pck1* and *G6pc* gene expression (*H*) were performed at 120 min after the intraperitoneal injection of histidine or saline (-) and glucose (2 g/kg body wt). $^*P < 0.05$ ($n = 5$). *I* and *J*: A fructose (*I*) and pyruvate (*J*) tolerance test was performed after the intraperitoneal administration of histidine or saline. $^*P < 0.05$ ($n = 10$). Cont, control.

by glucose loading (Fig. 1*G*). While the intraperitoneal administration of histidine alone did not significantly change blood glucose levels, it significantly downregulated the expression of the *G6pc* gene, which encodes G6Pase, with and without glucose loading (Fig. 1*H*). However, the expression of the *Pck1* gene, which encodes PEPCK, did not change significantly after the intraperitoneal administration of histidine alone or with glucose. The administration of fructose and pyruvate is known to increase blood glucose levels mildly through gluconeogenesis (20,21); however, histidine

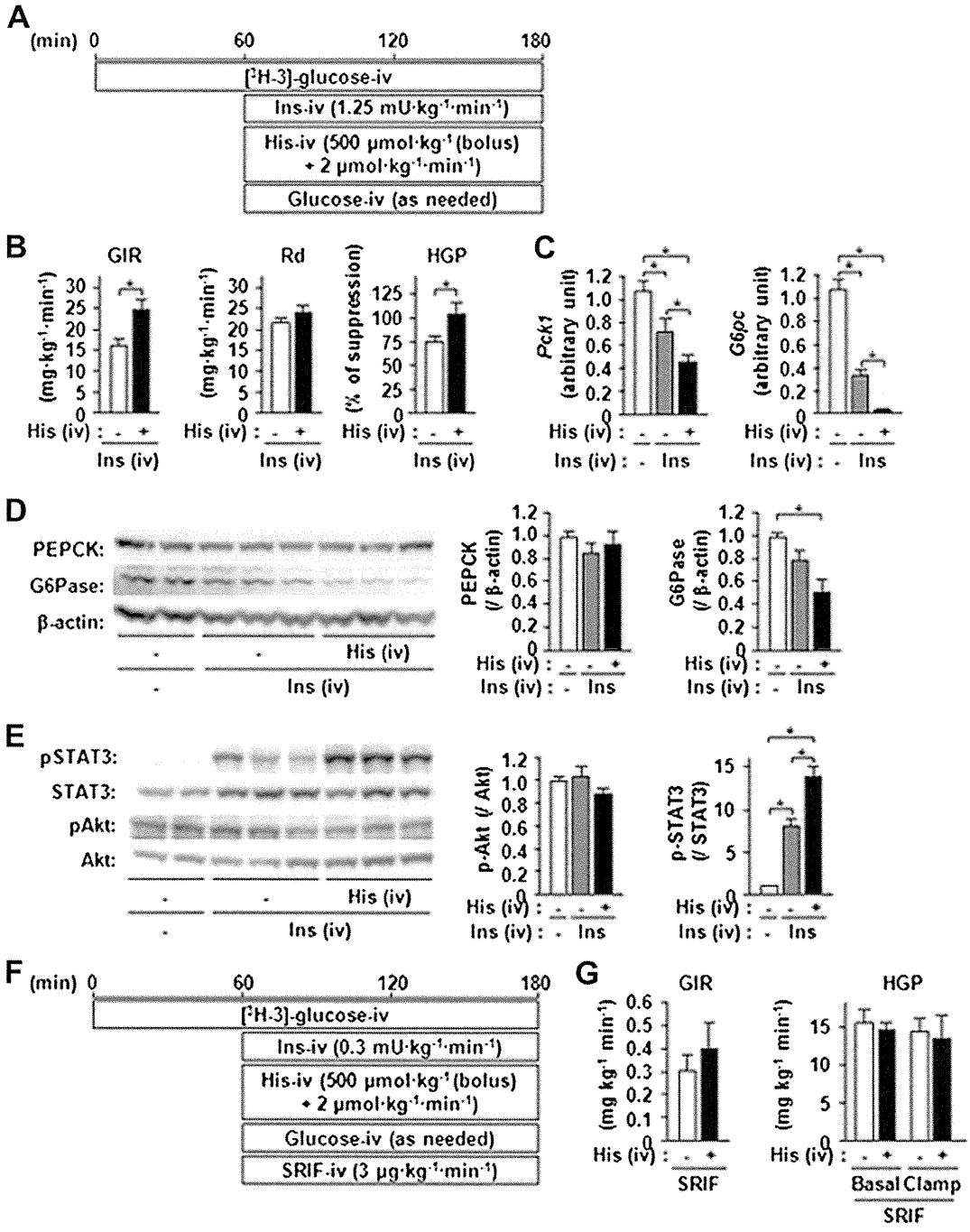

FIG. 2. Augmentation of the insulin-dependent suppression of HGP by histidine. *A*: Schematic of hyperinsulinemic-euglycemic clamping with continuous intravenous administration of histidine (His) or saline (-). *B* and *C*: GIR (*B*, *left panel*), R_d (*B*, *center panel*), and the suppression (%) of HGP (*B*, *right panel*) in the study described in *A*. Quantitative PCR analysis of *Pck1* and *G6pc* gene expression levels in the liver is shown in *C*. **P* < 0.05 (*n* = 7–9). *D* and *E*: Western blotting was performed to analyze the levels of hepatic PEPCK, G6Pase, and β-actin (*D*) and phosphorylation of STAT3 and Akt (*E*) at 120 min after insulin (Ins) administration in the hyperinsulinemic-euglycemic clamp study (*A*). Quantitation of PEPCK and G6Pase levels is normalized to β-actin (*D*). Quantitation of phospho-Akt and phospho-STAT3 is normalized to Akt and STAT3, respectively (*E*). Data are represented as means ± SE (*n* = 7–9) values. *F*: Schematic of euglycemic-pancreatic clamp tests with continuous intravenous administration of histidine or saline in addition to somatostatin injection. *G*: The GIR (*left panel*) and the suppression (%) of HGP (*right panel*) in the study described in *F* (*n* = 5).

injection attenuated the increase in blood glucose levels after the administration of fructose (Fig. 1*I*) and pyruvate (Fig. 1*J*).

Histidine administration augments the insulin-induced suppression of HGP. We used a hyperinsulinemic-euglycemic clamp technique to investigate the effect of histidine on HGP (Fig. 2*A*). The GIR and the suppression rate of HGP obtained after insulin administration were increased by histidine administration (Fig. 2*B*). The suppression of hepatic gene expression of *Pck1* and *G6pc* by insulin was augmented by histidine (Fig. 2*C*), even though histidine did not affect plasma insulin levels in the clamp tests (Supplementary Fig. 1). While PEPCK protein expression did not change significantly during the 120-min hyperinsulinemic-euglycemic clamping period, insulin administration reduced the levels of G6Pase protein, and this reduction was

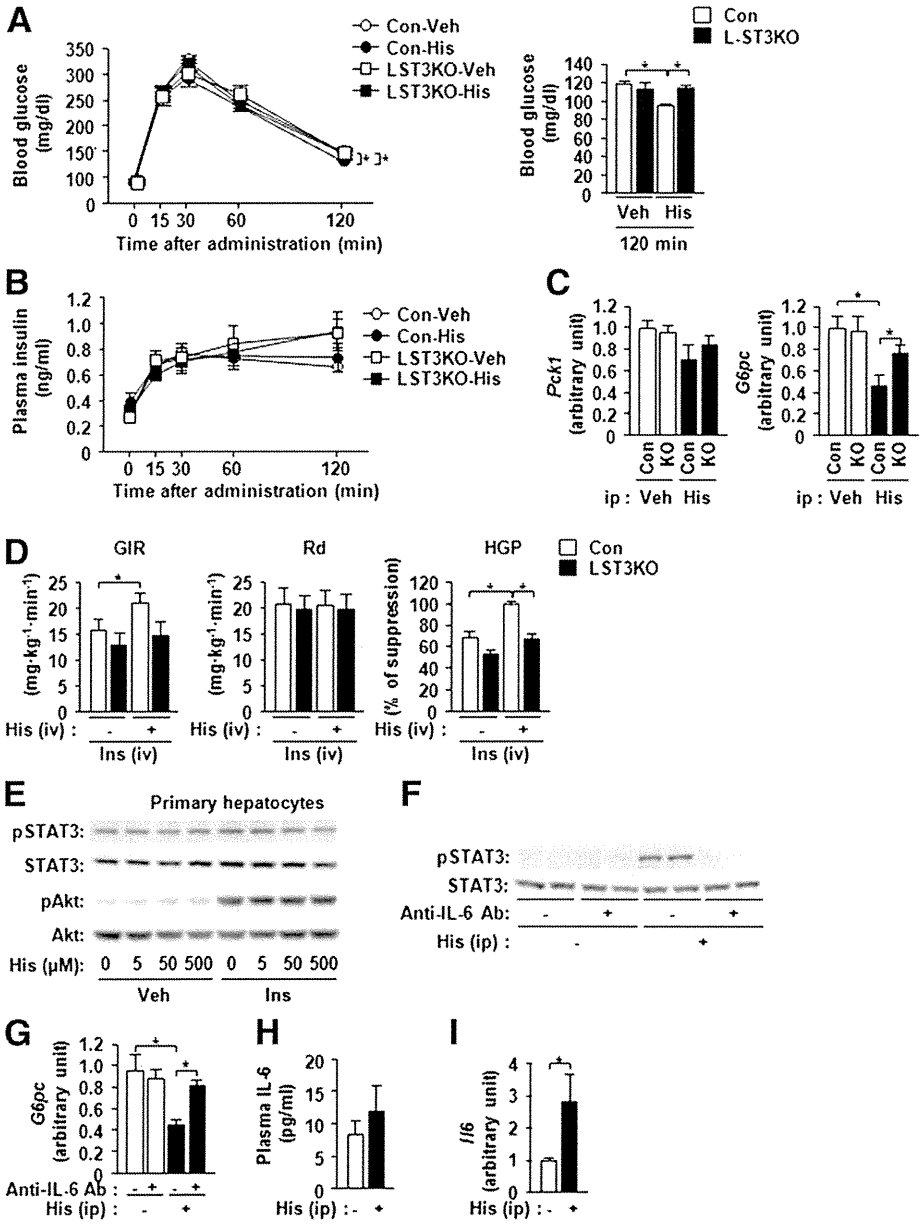

FIG. 3. Activation of hepatic IL-6/STAT3 signaling pathways is required for the histidine-mediated regulation of HGP. *A* and *B*: A glucose tolerance test was conducted after the intraperitoneal injection of histidine (His) in liver-specific STAT3-deficient (LST3KO) mice and controls (Con). Changes in blood glucose levels (*A*, *left panel*), blood glucose levels at 120 min after glucose loading (*A*, *right panel*), and changes in plasma insulin levels (*B*) are shown. *$P < 0.05$ ($n = 10$). *C*: Expression of hepatic *Pck1* and *G6pc* genes was analyzed by quantitative PCR at 120 min after the intraperitoneal injection of His into LST3KO and control (Con) mice. *$P < 0.05$ ($n = 6$–8). *D*: Hyperinsulinemic-euglycemic clamping was conducted as described in Fig. 2*A*. The GIR (*left panel*), R_d (*center panel*), and suppression (%) of HGP (*right panel*) were measured. *$P < 0.05$ ($n = 6$). *E*: Primary hepatocytes were treated with the different concentrations of histidine and insulin (Ins) shown in the figure, and the phosphorylation of STAT3, Akt, p70 S6 kinase, and S6 ribosomal protein was analyzed. *F*–*I*: The effect of intraperitoneal histidine injection on liver function was investigated using an IL-6 neutralizing antibody. *F*: Phosphorylation of hepatic STAT3 was analyzed by Western blotting at 120 min after histidine administration. *G*–*I*: Hepatic *G6pc* gene expression (*G*), blood IL-6 levels (*H*), and hepatic *Il6* gene expression (*I*) at 120 min after histidine administration are shown. *$P < 0.05$ ($n = 7$–9).

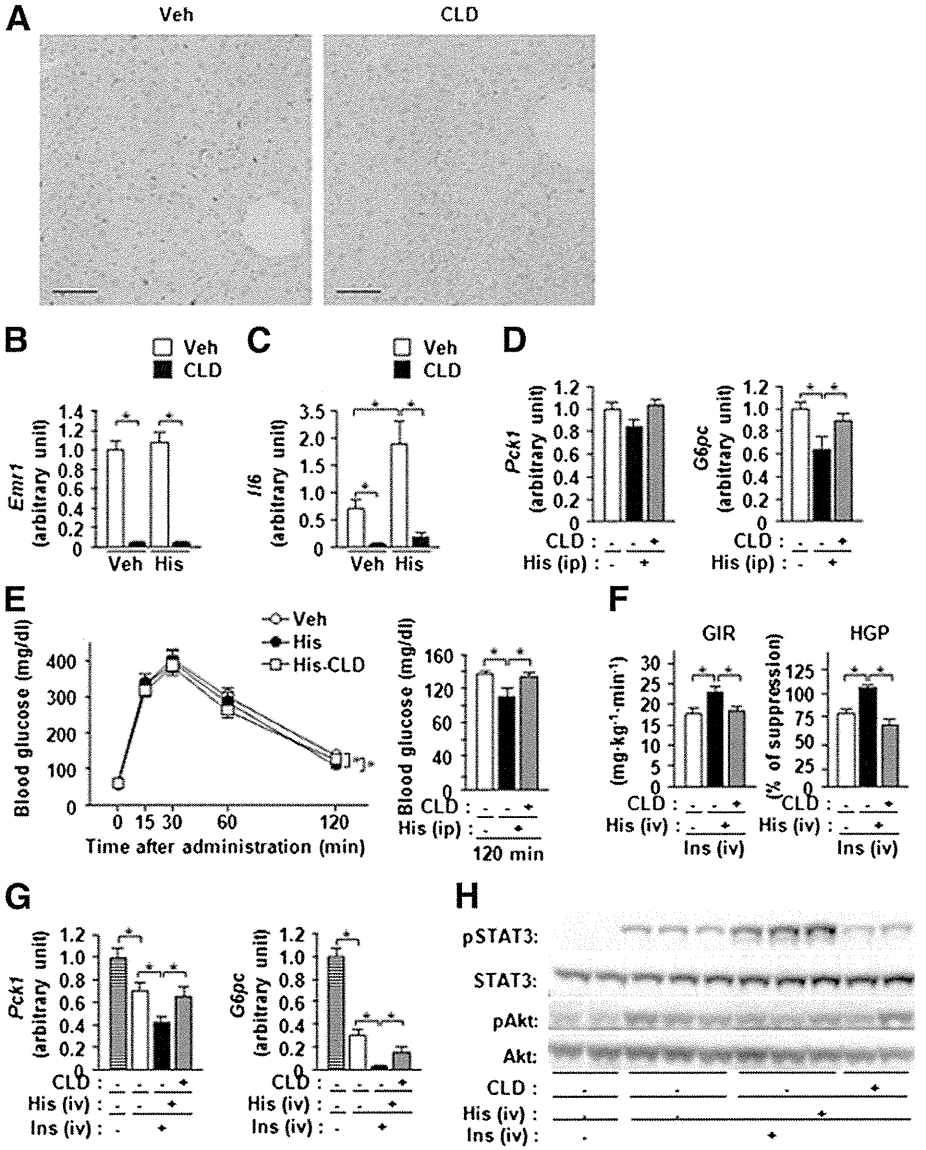

FIG. 4. Liver Kupffer cells are essential for the regulation of HGP by histidine (His). ***A*****: Immunostaining with an anti-Mac-2 antibody was performed in Kupffer cells after the administration of CLD. Scale bars, 50 nm.** ***B–D*****: Histidine was injected intraperitoneally into mice pretreated with CLD, and** ***Emr1*** **(*B*),** ***Il6*** **(*C*), and** ***Pck1*** **and** ***G6pc*** **(*D*) gene expression in the liver was quantitated using PCR at 120 min after histidine administration. *$P < 0.05$ ($n = 5–7$).** ***E*****: The intraperitoneal injection of histidine and a glucose tolerance test were conducted in mice pretreated with CLD. Changes in blood glucose levels (*E*, *left panel*) and blood glucose levels at 120 min after glucose loading (*E*, *right panel*) are shown. *$P < 0.05$ ($n = 9$).** ***F–H*****: With the continuous administration of histidine, hyperinsulinemic-euglycemic clamping (Fig. 2*A*) was performed in mice pretreated with CLD, and the GIR (*left panel*) and suppression (%) of HGP (*right panel*) were measured. In addition, the expression of hepatic** ***Pck1*** **and** ***G6pc*** **genes (*G*) and the phosphorylation of hepatic STAT3 and Akt (*H*) at 120 min after insulin (Ins) administration were examined. *$P < 0.05$ ($n = 6$).**

augmented by histidine administration (Fig. 2*D*). Phosphorylation of STAT3, but not Akt, was observed at 120 min after insulin administration (Fig. 2*E*), and histidine enhanced the phosphorylation of STAT3 caused by hyperinsulinemia (Fig. 2*E*). To evaluate the histidine effect of HGP with fasting levels of insulin, we performed euglycemic-pancreatic clamp tests (Fig. 2*F*). No significant changes in GIR or HGP resulted from the presence or absence of histidine injection (Fig. 2*G*).

Activation of hepatic IL-6/ STAT3 signaling pathways essential for the histidine-mediated regulation of hepatic glucose metabolism. We investigated the significance of hepatic STAT3 in the suppression of HGP after histidine administration using 8- to 10-week-old LST3KO mice, which had not yet developed insulin resistance (5). In a glucose tolerance test with histidine administration, blood glucose levels were significantly decreased in the control, but not LST3KO, mice at 120 min after glucose loading (Fig. 3*A*), even though no significant difference in plasma insulin levels was observed between the groups (Fig. 3*B*). While *G6pc* gene expression was downregulated at 120 min after the intraperitoneal administration of histidine in the control mice, no such downregulation was observed in the LST3KO mice (Fig. 3*C*). In the hyperinsulinemic-euglycemic clamp tests, histidine increased the GIR and the suppression of HGP caused by insulin administration

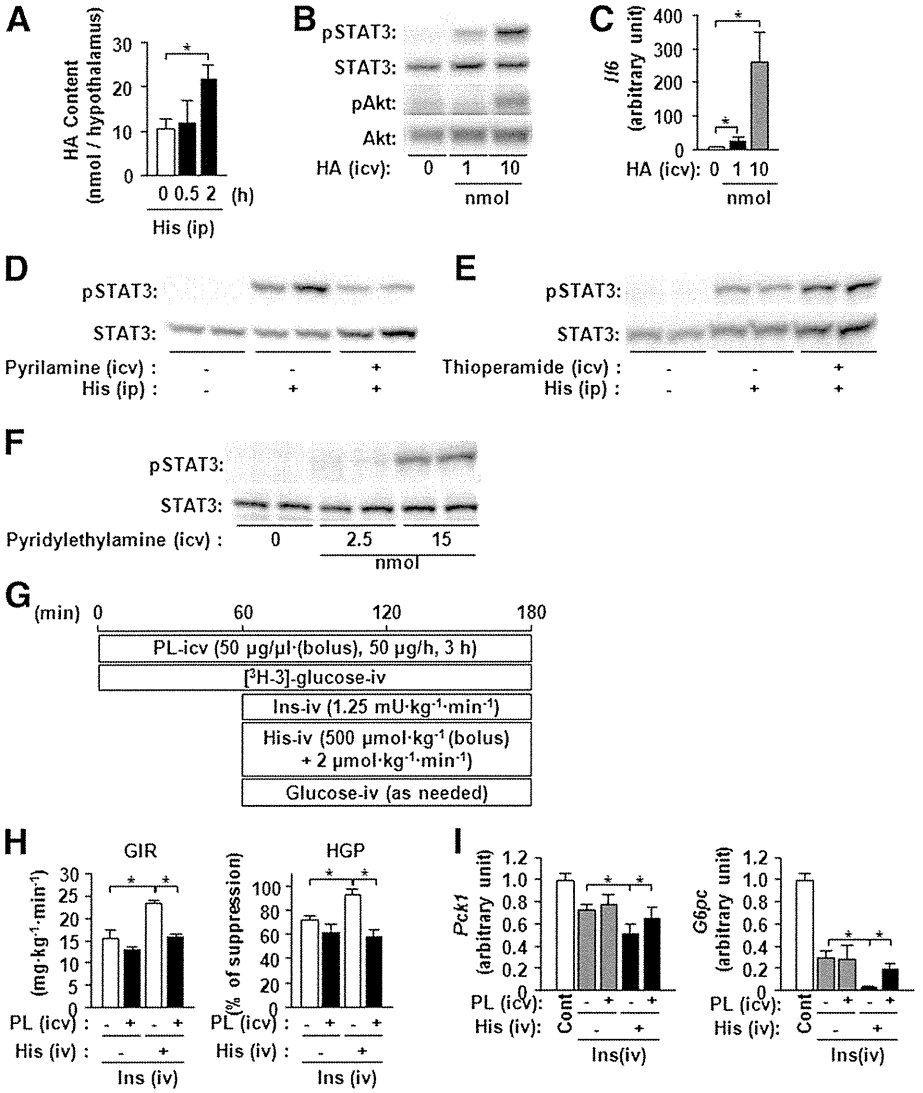

FIG. 5. Central histamine action is required for the regulation of HGP by histidine. *A*: Hypothalamic histamine (HA) content was measured at 30 and 120 min after the intraperitoneal administration of histidine (His). **P* < 0.05 (*n* = 5). *B* and *C*: HA was injected into the ventricle at the concentrations shown in the figure, and the phosphorylation of hepatic STAT3 and Akt (*B*) and expression of hepatic *Il6* gene (*C*) were analyzed at 180 min postadministration. **P* < 0.05 (*n* = 5). *D*: Histidine was injected intraperitoneally at 15 min after the lateral ventricular administration of the histamine H_1 receptor antagonist pyrilamine (50 μg/mouse), and phosphorylation of hepatic STAT3 was analyzed at 120 min after histidine administration. *E*: The intraperitoneal administration of histidine was performed at 30 min after the lateral ventricular administration of the histamine H_3 receptor antagonist thioperamide (50 nmol/mouse), and phosphorylation of hepatic STAT3 was analyzed at 120 min after histidine administration. *F*: Phosphorylation of hepatic STAT3 was analyzed (*n* = 4) at 180 min after the lateral ventricular administration of the histamine H_1 receptor agonist pyridylethylamine at the concentrations indicated in the figure. *G–I*: A hyperinsulinemic-euglycemic clamp (Ins injection) was performed with the continuous administration of histidine (His) or saline (-) in the jugular vein and pyrilamine (PL) or artificial cerebrospinal fluid (-) in the lateral ventricle, as shown in the schematic (*G*). The GIR (*H, left panel*) and the suppression (%) of HGP (*H, right panel*) are shown. ANOVA for GIR (*H, left panel*) revealed a significant effect of pyrilamine and histidine, as well as an interaction between pyrilamine and histidine ($P < 0.05$, $n = 6$). ANOVA for HGP (*H, right panel*) revealed a significant main effect of pyrilamine ($P < 0.05$) and an interaction between pyrilamine and histidine ($P < 0.01$, $n = 6$). In addition, the expression of hepatic *Pck1* and *G6pc* genes was analyzed at 120 min after insulin administration (*I*). **P* < 0.05 (*n* = 6). Cont, control.

in the control animals but not in the LST3KO mice (Fig. 3*D*). Insulin activates hepatic STAT3 via the central nervous system and the subsequent upregulation of *Il6* gene expression in the liver (9). Indeed, not only insulin but also histidine failed to activate STAT3 in primary hepatocytes (Fig. 3*E*). Histidine also had no effect on the Akt and S6 kinase pathway (Fig. 3*E*). Therefore, we used an IL-6 neutralizing antibody to investigate the role of IL-6 in the histidine-mediated activation of hepatic STAT3. The administration of the anti–IL-6 antibody prior to histidine administration attenuated the histidine-induced phosphorylation of STAT3 (Fig. 3*F*) as well as the suppression of *G6pc* gene expression (Fig. 3*G*). Histidine administration did not significantly change the plasma levels of IL-6 (Fig. 3*H*) but significantly upregulated *Il6* gene expression in the liver (Fig. 3*I*). These results suggest that, similar to insulin, histidine activates hepatic STAT3 through the upregulation of hepatic IL-6.

Kupffer cells are essential for the histidine-mediated regulation of hepatic glucose metabolism. In the liver, Kupffer cells play an important role in the production of

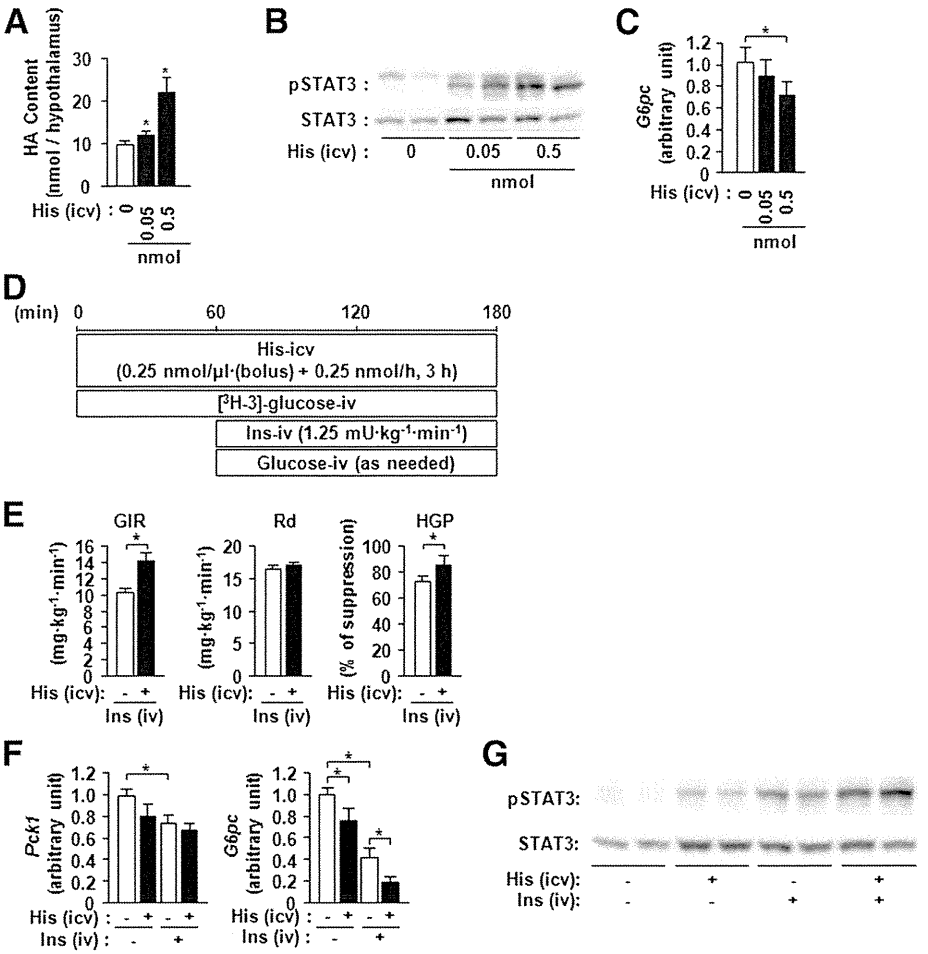

FIG. 6. ICV administration of histidine (His) augments the insulin-dependent suppression of HGP. *A–C*: With use of the doses indicated in the figure, histidine was injected rapidly into the lateral ventricle, and hypothalamic histamine (HA) content (*A*), phosphorylation of hepatic STAT3 (*B*), and expression of the hepatic *G6pc* gene (*C*) were analyzed at 180 min postadministration. *$P < 0.05$ (n = 5–8). *D–G*: As shown in the schematic (*D*), hyperinsulinemic-euglycemic clamping was performed concurrently with the continuous administration of histidine or artificial cerebrospinal fluid (-) into the lateral ventricle. The GIR (*E*, *left panel*), R_d (*E*, *center panel*), and suppression (%) of HGP (*E*, *right panel*) were measured. *$P < 0.05$ (n = 6). In addition, the expression of hepatic *Pck1* and *G6pc* genes (*F*) and phosphorylation of hepatic STAT3 (*G*) were analyzed at 120 min after insulin administration. ANOVA for *Pck1* (*F*, *left panel*) revealed a significant main effect of Ins ($P < 0.05$) but no significant interaction between Ins and His (P = 0.060, n = 6). ANOVA for *G6pc* (*F*, *right panel*) revealed a significant main effect of Ins and histidine ($P < 0.05$), but no significant interaction between insulin and histidine treatments (P = 0.120, n = 6).

IL-6 (22,23); therefore, we depleted Kupffer cells by the intravenous injection of CLD and investigated the function of histidine (22). CLD administration resulted in the disappearance of Mac-2–positive cells (Fig. 4*A*) and significantly downregulated the expression of the *Emr1* gene (Fig. 4*B*), which is specific to Kupffer cells in the liver. In addition, the depletion of Kupffer cells diminished the expression of hepatic *Il6* (Fig. 4*C*). Histidine administration, which significantly downregulates the expression of the hepatic *G6pc* gene, did not change its expression after CLD administration (Fig. 4*D*). In the glucose tolerance test, histidine administration significantly reduced blood glucose levels at 120 min after glucose loading; however, this reduction was diminished after CLD administration (Fig. 4*E*). In a hyperinsulinemic-euglycemic clamp experiment, histidine augmented the effects of insulin on *Pck1* and *G6pc* gene expression, HGP, and the GIR, but the augmentation of insulin action by histidine was diminished by CLD administration (Fig. 4*F* and *G*). Although histidine augmented the STAT3 phosphorylation caused by hyperinsulinemia, this augmentation was attenuated by CLD administration (Fig. 4*H*). These results indicate that hepatic IL-6 expression in Kupffer cells is essential for the histidine-mediated regulation of hepatic glucose metabolism.

Central histamine mediates the regulation of hepatic glucose metabolism by histidine. Histidine is a precursor of histamine; therefore, the levels of histamine in the hypothalamus are reportedly increased after the systemic administration of histidine (24,25). Thus, we investigated the involvement of central histamine in the histidine-mediated activation of hepatic STAT3 and regulation of HGP. As reported previously, histidine administration increased the levels of histamine in the hypothalamus (Fig. 5*A*). In addition, the ICV administration of histamine induced the phosphorylation of hepatic STAT3 (Fig. 5*B*) and upregulated the expression of *Il6* in the liver (Fig. 5*C*). The lateral ventricular administration of the histamine H_1 receptor antagonist pyrilamine prior to systemic histidine administration attenuated the phosphorylation of hepatic STAT3 (Fig. 5*D*), whereas the ICV administration of the histamine

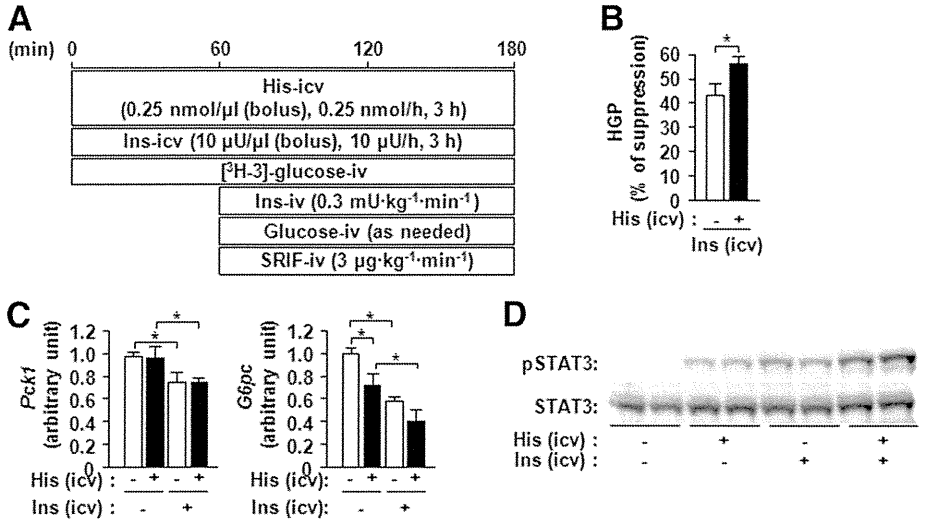

FIG. 7. Central histidine (His) action augments the suppression of HGP by insulin ICV administration. ***A–D*****: As shown in the schematic (*A*), continuous lateral ventricular injection of histidine, artificial cerebrospinal fluid (aCSF) (-), and insulin (Ins) in pancreatic clamping was performed. The suppression (%) of HGP, *$P < 0.05$ ($n = 6$) (*B*), expression of hepatic *Pck1* and *G6pc* genes at 180 min after the start of lateral ventricular administration (*C*), and phosphorylation of hepatic STAT3 (*D*) were analyzed. ANOVA for *Pck1* expression (*C, left panel*) revealed a significant main effect of Ins ($P < 0.05$) but no significant interaction between insulin and histidine ($P = 0.964$, $n = 6$). ANOVA for *G6pc* expression (*C, right panel*) revealed a significant main effect of insulin and histidine ($P < 0.05$) but no significant interaction between insulin and histidine treatments ($P = 0.116$, $n = 6$).**

H3 receptor antagonist thioperamide increased STAT3 phosphorylation (Fig. 5*E*). Conversely, the ICV administration of the histamine H_1 receptor agonist pyridylethylamine activated hepatic STAT3 (Fig. 5*F*). To elucidate the role of central histamine/histamine H_1 receptor in the histidine-mediated regulation of HGP, we performed a hyperinsulinemic-euglycemic clamp study with the concurrent ICV administration of pyrilamine and intravenous administration of histidine (Fig. 5*G*). Although histidine administration augmented the action of insulin on *Pck1* and *G6pc* gene expression, HGP, and the GIR, the ICV administration of pyrilamine blocked this augmentation (Fig. 5*H* and *I*).

ICV administration of histidine augments the insulin-dependent suppression of HGP. We administered histidine into the ventricle to investigate the involvement of the central-mediated regulation of HGP by histidine. As with intraperitoneal injection, the ICV administration of histidine increased the hypothalamic histamine content (Fig. 6*A*). In addition, histidine ICV administration upregulated the phosphorylation of hepatic STAT3 (Fig. 6*B*) and suppressed *G6pc* gene expression in the liver (Fig. 6*C*). We then investigated the effect of histidine ICV administration on the insulin-dependent suppression of HGP (Fig. 6*D*). In hyperinsulinemic-euglycemic clamping, the ICV administration of histidine increased the GIR and augmented the suppression of HGP (Fig. 6*E*). The ICV administration of histidine suppressed the expression of the *G6pc* gene and augmented the suppression of gene expression by the systemic administration of insulin (Fig. 6*F*), whereas *Pck1* gene expression tended to decrease, albeit insignificantly, after histidine administration (Fig. 6*F*). Furthermore, histidine ICV administration increased the phosphorylation of hepatic STAT3 and additively enhanced the hepatic phosphorylation of STAT3 associated with hyperinsulinemia (Fig. 6*G*). These results indicate that the suppression of HGP by the systemic administration of insulin is augmented by the central administration of histidine.

We then injected insulin and histidine into the ventricle to investigate the effect of central histidine on the regulation of HGP by central insulin action (Fig. 7*A*). The ICV administration of insulin was performed with the concurrent administration of somatostatin to block the secretion of endogenous insulin caused by insulin ICV administration (Fig. 7*A*). As reported previously, the ICV administration of insulin suppressed HGP, while the ICV administration of histidine augmented this suppression (Fig. 7*B*). In addition, with the ICV administration of insulin the expression of the *Pck1* gene decreased, albeit insignificantly, whereas the expression of the *G6pc* gene was significantly down-regulated (Fig. 7*C*). Histidine administration augmented the suppression of *G6pc* gene expression (Fig. 7*C*). Hepatic STAT3 was phosphorylated after the ICV administration of insulin or histidine, and their coadministration enhanced its phosphorylation (Fig. 7*D*). These results indicate that the central administration of histidine augments the suppression of HGP by central insulin action.

Central histidine action is independent of central insulin action. Next, we investigated the cross-talk between central histidine and central insulin action, both of which activate hepatic STAT3. As pyrilamine administration inhibited hepatic STAT3 phosphorylation mediated by the systemic administration of histidine (Fig. 5*D*), the phosphorylation of hepatic STAT3 was attenuated by the administration of pyrilamine prior to the ICV administration of histidine (Fig. 8*A*). Conversely, the phosphorylation of hepatic STAT3 induced by the ICV administration of insulin was not altered by the preadministration of pyrilamine (Fig. 8*B*). Furthermore, in a study using Hrh1KO mice (16) the phosphorylation of hepatic STAT3 was significantly attenuated after the ICV administration of histidine (Fig. 8*C*) in the same manner as that after pyrilamine administration. However, no significant change in hepatic STAT3 phosphorylation was induced by the ICV administration of insulin to the Hrh1KO mice (Fig. 8*D*).

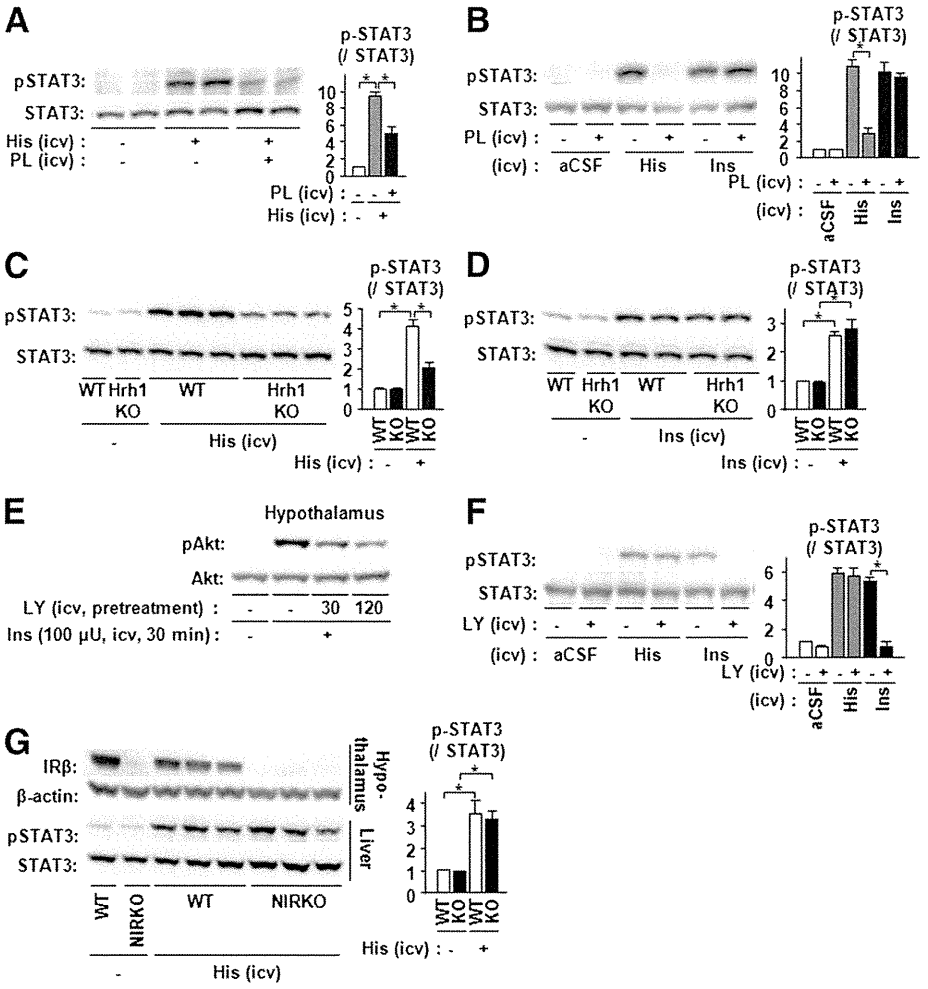

FIG. 8. Central histidine (His) action on the liver is independent of central insulin (Ins) action. *A* **and** *B*: **Phosphorylation of STAT3 was analyzed at 180 min after the intravenous administration of somatostatin (3 μg · kg^{-1} · min^{-1}) and the lateral ventricular administration of histidine (*A* and *B*) or insulin (*B*), which was performed at 15 min after the ICV preadministration of the histamine H_1 antagonist pyrilamine (50 μg/mouse). Quantitation is represented as means ± SE (*n* = 6–8).** *C* **and** *D*: **Somatostatin administration (3 μg · kg^{-1} · min^{-1}) and the lateral ventricular administration of histidine (*C*) or insulin (*D*) were performed in Hrh1KO mice, and the phosphorylation of hepatic STAT3 was analyzed at 180 min postadministration. Quantitation is represented as means ± SE (*n* = 6).** *E*: **The ICV administration of insulin (100 μU/mouse, bolus) was performed at 30 and 120 min after the administration of the PI3-K inhibitor LY294002 (10 nmol/mouse; LY). The phosphorylation of hypothalamic Akt at 30 min after insulin administration is shown.** *F*: **Somatostatin administration (3 μg · kg^{-1} · min^{-1}) and the lateral ventricular administration of histidine or insulin were performed at 120 min after the lateral ventricular administration of LY294002 (10 nmol/mouse; LY), and the phosphorylation of hepatic STAT3 was analyzed at 180 min postadministration. Quantitation is represented as means ± SE (*n* = 5).** *G*: **Somatostatin (3 μg · kg^{-1} · min^{-1}) and histidine were administered into NIRKO mice, and the levels of hypothalamic insulin receptor (IRβ), β-actin, and hepatic STAT3 were analyzed at 180 min postadministration. Quantitation is represented as means ± SE (*n* = 6). aCSF, artificial cerebrospinal fluid; WT, wild type.**

Insulin-dependent phosphorylation of hypothalamic Akt was attenuated by the ICV administration of the PI3-K inhibitor LY294002 (Fig. 8*E*). We therefore investigated the effect of the ICV administration of histidine or insulin, with the concurrent administration of LY294002, on the phosphorylation of hepatic STAT3. LY294002 inhibited the insulin-induced phosphorylation of hepatic STAT3 but did not affect its phosphorylation by histidine (Fig. 8*F*). We also examined mice lacking central insulin receptors. In the NIRKO mice, as in the control mice, the ICV administration of histidine induced hepatic STAT3 phosphorylation (Fig. 8*G*). These results suggest that central histidine action mediated by the histamine H_1 receptor is independent of central insulin action but that they function additively to suppress HGP.

DISCUSSION

The central nervous system monitors hormonal and nutritional changes that regulate energy metabolism in peripheral tissues. In this study, we revealed that an increase in blood histidine levels acts on the central nervous system, activates hepatic IL-6/STAT3 signaling, suppresses the expression of gluconeogenic genes in the liver, and augments the insulin-dependent suppression of HGP. These findings suggest that histidine can be a target molecule for the treatment of type 2 diabetes. Recently, plasma histidine levels were reported to show a significant inverse association with fasting and 2-h blood glucose levels during glucose tolerance tests in individuals without diabetes or newly diagnosed male patients with type 2 diabetes (14). Histidine was also shown to improve the hyperglycemia induced by

the central administration of 2-deoxyglucose in rodents (26); however, the mechanism by which histidine lowers blood glucose levels is not clear. In the current study, the intraperitoneal administration of histidine induced the phosphorylation of hepatic STAT3 and reduced blood glucose levels associated with glucose loading. Consistent with a previous study showing that histidine is not involved in the secretion of insulin (27), histidine did not significantly affect plasma insulin levels in the current study. In the hyperinsulinemic-euglycemic clamp experiment, the intravenous administration of histidine increased GIR and the suppression of HGP. Such histidine action was not observed in LST3KO mice or Kupffer cell–depleted mice, suggesting that the activation of hepatic IL-6/STAT3 signaling plays an important role in the histidine-mediated suppression of HGP. The gene expression of *G6pc* and *Pck1* was downregulated by histidine administration in the hyperinsulinemic-euglycemic clamp experiment, with a clear reduction in the protein levels of G6Pase but not PEPCK. These findings suggest that the downregulation of G6Pase expression causes the suppression of HGP by histidine. However, the activation of hepatic STAT3 by histidine alone is relatively weak, resulting in the mild suppression of *G6pc* gene expression but not of *Pck1*. Furthermore, euglycemic-pancreatic clamp tests with histidine did not reveal a significant change in HGP. These findings may explain why histidine administration alone is not enough to affect the homeostasis of blood glucose levels.

In the brain, histidine is converted into histamine by histidine decarboxylase in the tuberomammillary nucleus of the posterior hypothalamus (24,25,28). Consistent with a previous study (25), hypothalamic histamine content was increased by histidine administration in the current study. A previous study using rats showed that enhanced central histamine action due to histidine administration suppresses food intake (25). In contrast, both Hrh1KO mice (29) and histidine decarboxylase knockout mice (30) present with insulin resistance as well as obesity. In addition, the development of obesity and diabetes caused by the antipsychotic drug olanzapine in humans is reportedly linked to inhibition of the histamine H_1 receptor (31). Such phenotypes may indicate that the action of histamine affects not only food intake but also glucose metabolism. In this study, the central administration of histamine H_1 receptor antagonist attenuated the activation of hepatic STAT3 and the suppression of HGP induced by the systemic administration of histidine. Furthermore, the central administration of histidine also activated hepatic STAT3 while suppressing HGP. These findings indicate that the histidine-induced suppression of HGP, as well as the suppression of food intake, is mediated by central histamine action. Because the histamine-containing neurons in the tuberomammillary nucleus project into most of the brain (28), the precise mechanism in the brain by which central histamine activates hepatic STAT3 remains unclear. This histidine action is additive to the insulin-induced suppression of HGP. The activation of hepatic STAT3 by central insulin action was not blocked by the central administration of a histamine H_1 receptor antagonist or in Hrh1KO mice. In contrast, the activation of hepatic STAT3 by central histidine was not blocked by the central administration of a PI3-K inhibitor or in NIRKO mice, suggesting that the mechanism underlying the action of central histidine is independent of insulin action.

This study demonstrates that the activation of hepatic IL-6/STAT3 signaling pathways and downregulation of hepatic gluconeogenic gene expression by histidine are mediated by central histamine action involving the histamine H_1 receptor. Central histidine action, which has a central nervous system mechanism that is independent of insulin, augments the insulin-dependent suppression of glucose production in the liver. This study indicates that the central mechanism by which histidine regulates hepatic glucose metabolism and activates hepatic STAT3 is a potential target for the treatment of type 2 diabetic patients with elevated gluconeogenesis.

ACKNOWLEDGMENTS

This work was supported by the Program for Promotion of Basic and Applied Research for Innovations in Bio-oriented Industry to H.I.; Ministry of Education, Culture, Sports, Science and Technology MEXT KAKENHI Grant 23126509 to H.I.; and Japan Society for the Promotion of Science KAKENHI grants 23300274 to H.I. and 24790919 to K.K.

ThinkSCIENCE, Inc. (Tokyo, Japan), assisted with manuscript preparation. No other potential conflicts of interest relevant to this article were reported.

K.K., Y.N., Y.I., S.As., T.M., H.W., A.M., and F.I. produced the data. M.M., T.O., and H.N. produced the data and contributed to the discussion. Y.K., C.M., K.T., S.Ak., and S.K. contributed to the discussion. M.K. contributed to the discussion and reviewed and edited the manuscript. H.I. researched the data, designed the study, contributed to the discussion, and wrote the manuscript. H.I. is the guarantor of this work and, as such, had full access to all the data in the study and takes responsibility for the integrity of the data and the accuracy of the data analysis.

The authors thank C.R. Kahn (Harvard Medical School) for NIRKO mice; H. Nakamura (Kanazawa University) for expert advice on the statistical analysis; and Y. Anraku, M. Nishio, and C. Asahi (Kanazawa University) for technical assistance.

REFERENCES

1. Magnusson I, Rothman DL, Katz LD, Shulman RG, Shulman GI. Increased rate of gluconeogenesis in type II diabetes mellitus. A ^{13}C nuclear magnetic resonance study. J Clin Invest 1992;90:1323–1327
2. Radziuk J, Pye S. Hepatic glucose uptake, gluconeogenesis and the regulation of glycogen synthesis. Diabetes Metab Res Rev 2001;17:250–272
3. Dentin R, Hedrick S, Xie J, Yates J 3rd, Montminy M. Hepatic glucose sensing via the CREB coactivator CRTC2. Science 2008;319:1402–1405
4. Rodgers JT, Haas W, Gygi SP, Puigserver P. Cdc2-like kinase 2 is an insulin-regulated suppressor of hepatic gluconeogenesis. Cell Metab 2010;11:23–34
5. Inoue H, Ogawa W, Ozaki M, et al. Role of STAT-3 in regulation of hepatic gluconeogenic genes and carbohydrate metabolism in vivo. Nat Med 2004;10:168–174
6. Kimura K, Yamada T, Matsumoto M, et al. Endoplasmic reticulum stress inhibits STAT3-dependent suppression of hepatic gluconeogenesis via dephosphorylation and deacetylation. Diabetes 2012;61:61–73
7. Lam TK. Neuronal regulation of homeostasis by nutrient sensing. Nat Med 2010;16:392–395
8. Cota D, Proulx K, Seeley RJ. The role of CNS fuel sensing in energy and glucose regulation. Gastroenterology 2007;132:2158–2168
9. Inoue H, Ogawa W, Asakawa A, et al. Role of hepatic STAT3 in brain-insulin action on hepatic glucose production. Cell Metab 2006;3:267–275
10. Obici S, Zhang BB, Karkanias G, Rossetti L. Hypothalamic insulin signaling is required for inhibition of glucose production. Nat Med 2002;8:1376–1382
11. Pocai A, Obici S, Schwartz GJ, Rossetti L. A brain-liver circuit regulates glucose homeostasis. Cell Metab 2005;1:53–61
12. Lam TK, Gutierrez-Juarez R, Pocai A, Rossetti L. Regulation of blood glucose by hypothalamic pyruvate metabolism. Science 2005;309:943–947

13. Obici S, Feng Z, Morgan K, Stein D, Karkanias G, Rossetti L. Central administration of oleic acid inhibits glucose production and food intake. Diabetes 2002;51:271–275
14. Stancáková A, Civelek M, Saleem NK, et al. Hyperglycemia and a common variant of GCKR are associated with the levels of eight amino acids in 9,369 Finnish men. Diabetes 2012;61:1895–1902
15. Su Y, Lam TK, He W, et al. Hypothalamic leucine metabolism regulates liver glucose production. Diabetes 2012;61:85–93
16. Inoue I, Yanai K, Kitamura D, et al. Impaired locomotor activity and exploratory behavior in mice lacking histamine H1 receptors. Proc Natl Acad Sci USA 1996;93:13316–13320
17. Brüning JC, Gautam D, Burks DJ, et al. Role of brain insulin receptor in control of body weight and reproduction. Science 2000;289:2122–2125
18. Nuttall FQ, Mooradian AD, Gannon MC, Billington C, Krezowski P. Effect of protein ingestion on the glucose and insulin response to a standardized oral glucose load. Diabetes Care 1984;7:465–470
19. Semon BA, Leung PM, Rogers QR, Gietzen DW. Increase in plasma ammonia and amino acids when rats are fed a 44% casein diet. Physiol Behav 1988;43:631–636
20. Miyake K, Ogawa W, Matsumoto M, Nakamura T, Sakaue H, Kasuga M. Hyperinsulinemia, glucose intolerance, and dyslipidemia induced by acute inhibition of phosphoinositide 3-kinase signaling in the liver. J Clin Invest 2002;110:1483–1491
21. Kyriazis GA, Soundarapandian MM, Tyrberg B. Sweet taste receptor signaling in beta cells mediates fructose-induced potentiation of glucose-stimulated insulin secretion. Proc Natl Acad Sci USA 2012;109: E524–E532
22. Van Rooijen N, Sanders A. Kupffer cell depletion by liposome-delivered drugs: comparative activity of intracellular clodronate, propamidine, and ethylenediaminetetraacetic acid. Hepatology 1996;23:1239–1243
23. Salkowski CA, Neta R, Wynn TA, Strassmann G, van Rooijen N, Vogel SN. Effect of liposome-mediated macrophage depletion on LPS-induced cytokine gene expression and radioprotection. J Immunol 1995;155:3168–3179
24. Anderson GH. Diet, neurotransmitters and brain function. Br Med Bull 1981;37:95–100
25. Yoshimatsu H, Chiba S, Tajima D, Akehi Y, Sakata T. Histidine suppresses food intake through its conversion into neuronal histamine. Exp Biol Med (Maywood) 2002;227:63–68
26. Nagai K, Niijima A, Yamano T, et al. Possible role of L-carnosine in the regulation of blood glucose through controlling autonomic nerves. Exp Biol Med (Maywood) 2003;228:1138–1145
27. Floyd JC Jr, Fajans SS, Conn JW, Knopf RF, Rull J. Stimulation of insulin secretion by amino acids. J Clin Invest 1966;45:1487–1502
28. Haas H, Panula P. The role of histamine and the tuberomamillary nucleus in the nervous system. Nat Rev Neurosci 2003;4:121–130
29. Masaki T, Chiba S, Yasuda T, et al. Involvement of hypothalamic histamine H1 receptor in the regulation of feeding rhythm and obesity. Diabetes 2004; 53:2250–2260
30. Fülöp AK, Földes A, Buzás E, et al. Hyperleptinemia, visceral adiposity, and decreased glucose tolerance in mice with a targeted disruption of the histidine decarboxylase gene. Endocrinology 2003;144:4306–4314
31. Deng C, Weston-Green K, Huang XF. The role of histaminergic H1 and H3 receptors in food intake: a mechanism for atypical antipsychotic-induced weight gain? Prog Neuropsychopharmacol Biol Psychiatry 2010;34:1–4

JVI
Journals.ASM.org

MicroRNA-27a Regulates Lipid Metabolism and Inhibits Hepatitis C Virus Replication in Human Hepatoma Cells

Takayoshi Shirasaki,[a,b] Masao Honda,[a,b] Tetsuro Shimakami,[a] Rika Horii,[a] Taro Yamashita,[a] Yoshio Sakai,[a] Akito Sakai,[a] Hikari Okada,[a] Risa Watanabe,[b] Seishi Murakami,[a] MinKyung Yi,[c] Stanley M. Lemon,[d] Shuichi Kaneko[a]

Department of Gastroenterology, Kanazawa University Graduate School of Medical Science, Kanazawa, Japan[a]; Department of Advanced Medical Technology, Kanazawa University Graduate School of Health Medicine, Kanazawa, Japan[b]; Human Center for Hepatitis Research, Institute for Human Infections and Immunity, and Department of Microbiology and Immunology, University of Texas Medical Branch, Galveston, Texas, USA[c]; Division of Infectious Diseases, School of Medicine, The University of North Carolina at Chapel Hill, Chapel Hill, North Carolina, USA[d]

The replication and infectivity of the lipotropic hepatitis C virus (HCV) are regulated by cellular lipid status. Among differentially expressed microRNAs (miRNAs), we found that miR-27a was preferentially expressed in HCV-infected liver over hepatitis B virus (HBV)-infected liver. Gene expression profiling of Huh-7.5 cells showed that miR-27a regulates lipid metabolism by targeting the lipid synthetic transcription factor RXRα and the lipid transporter ATP-binding cassette subfamily A member 1. In addition, miR-27a repressed the expression of many lipid metabolism-related genes, including *FASN*, *SREBP1*, *SREBP2*, *PPARα*, and *PPARγ*, as well as *ApoA1*, *ApoB100*, and *ApoE3*, which are essential for the production of infectious viral particles. miR-27a repression increased the cellular lipid content, decreased the buoyant density of HCV particles from 1.13 to 1.08 g/cm^3, and increased viral replication and infectivity. miR-27a overexpression substantially decreased viral infectivity. Furthermore, miR-27a enhanced *in vitro* interferon (IFN) signaling, and patients who expressed high levels of miR-27a in the liver showed a more favorable response to pegylated IFN and ribavirin combination therapy. Interestingly, the expression of miR-27a was upregulated by HCV infection and lipid overload through the adipocyte differentiation transcription factor C/EBPα. In turn, upregulated miR-27a repressed HCV infection and lipid storage in cells. Thus, this negative feedback mechanism might contribute to the maintenance of a low viral load and would be beneficial to the virus by allowing it to escape host immune surveillance and establish a persistent chronic HCV infection.

MicroRNA (miRNA) is a small, endogenous, single-stranded, noncoding RNA consisting of 20 to 25 bases that regulates gene expression. It plays an important role in various biological processes, including organ development, differentiation, and cellular death and proliferation, and is also involved in infection and diseases such as cancer (1).

Previously, we examined miRNA expression in hepatocellular carcinoma (HCC) and noncancerous background liver tissue infected with hepatitis B virus (HBV) and HCV (2). We showed that some miRNAs were differentially expressed according to HBV or HCV infection but not according to the presence of HCC. These infection-specific miRNAs were believed to regulate HBV or HCV replication; however, their functional role has not been elucidated.

HCV is described as a lipotropic virus because of its association with serum lipoprotein (3–5). It utilizes the low-density lipoprotein (LDL) receptor for cellular entry (6–8) and forms replication complexes on lipid rafts (9). The HCV core protein surrounds and binds lipid droplets (LDs) and nonstructural proteins on the endoplasmic reticulum (ER) membrane, which is essential for particle formation (10). Moreover, HCV cellular secretion is linked to very LDL (VLDL) secretion (11). In liver tissue histology, steatosis is often observed in chronic hepatitis C (CH-C) and is closely related to resistance to interferon (IFN) treatment (12, 13). Thus, lipids play important roles in HCV replication and CH-C pathogenesis.

Several miRNAs, such as miR-122 (14), miR-199a (15), miR-196 (16), miR-29 (17), Let-7b (18), and miR-130a (19), reportedly regulate HCV replication; however, miRNAs that regulate lipid metabolism and HCV replication have not been reported so far. Previously, we reported that 19 miRNAs were differentially expressed in HBV- and HCV-infected livers (2). In the present study, we evaluated the functional relevance of miR-27a in HCV replication by using the human hepatoma cell line Huh-7.5. We analyzed the regulation of lipid metabolism by miR-27a in hepatocytes and revealed a unique pathophysiological relationship between lipid metabolism and HCV replication in CH-C.

MATERIALS AND METHODS

Cell line. Huh-7.5 cells (kindly provided by C. M. Rice, Rockefeller University, New York, NY) were maintained in Dulbecco's modified Eagle's medium (DMEM; Gibco BRL, Gaithersburg, MD) containing 10% fetal bovine serum (FBS) and 1% penicillin-streptomycin.

HCV replication analysis. HCV replication analysis was performed by transfecting Huh-7.5 cells with JFH-1 (20), H77Sv2 Gluc2A (21), and their derivative RNA constructs. pH77Sv2 is a modification of pH77S, a plasmid containing the full-length sequence of the genotype 1a H77 HCV strain with five cell culture-adaptive mutations that promote its replication in Huh-7 hepatoma cells (21–24). pH77Sv2 Gluc2A is a related construct in which the *Gaussia* luciferase (Gluc) sequence, fused to the 2A autocatalytic protease of foot-and-mouth virus RNA, was inserted in frame between p7 and NS2 (21, 23, 25). pH77Sv2 Gluc2A (AAG) is a control plasmid that has an NS5B polymerase catalytic domain mutation.

Received 29 October 2012 Accepted 21 February 2013
Published ahead of print 28 February 2013
Address correspondence to Masao Honda, mhonda@m-kanazawa.jp.

doi:10.1128/JVI.03022-12

For RNA transfection, the cells were washed with phosphate-buffered saline (PBS) and resuspended in complete growth medium. The cells were then pelleted by centrifugation (1,400 × *g* for 4 min at 4°C), washed twice with ice-cold PBS, and resuspended in ice-cold PBS at a concentration of 7.5×10^6 cells/0.4 ml. The cells were mixed with 10 μg of the RNA transcripts, placed into 2-mm-gap electroporation cuvettes (BTX Genetronics, San Diego, CA), and electroporated with five pulses of 99 μs at 750 V over 1.1 s in an ECM 830 (BTX Genetronics). Following a 10-min recovery period, the cells were mixed with complete growth medium and plated.

miR-27a and anti-miR-27a transfection. Huh-7.5 cells transfected with pH77Sv2 Gluc2A RNA or pH77Sv2 Gluc2A (AAG) RNA were transfected with 50 nM synthetic miRNA (pre-miRNA) or 50 nM anti-miRNA (Ambion Inc., Austin, TX) with the siPORTTM NeoFXTM Transfection Agent (Ambion). Transfection was performed immediately by mixing the electroporated cells with the miRNA transfection reagents. Control samples were transfected with an equal concentration of a nontargeting control (pre-miRNA negative control) or inhibitor negative control (anti-miRNA negative control) to assess non-sequence-specific effects in the miRNA experiments.

Fatty acid treatment. Huh-7.5 cells transfected with HCV RNA and pre- or anti-miRNA were cultured for 24 h and then treated with the indicated concentrations of oleic acid (0 to 250 μM) (26) in the presence of 2% free fatty acid (FFA)-free bovine serum albumin (BSA; Sigma-Aldrich, St. Louis, MO). The cells were harvested at 72 h posttreatment with oleic acid for quantitative real-time detection PCR (RTD-PCR), Western blotting, immunofluorescence staining, and reporter analysis. The number of viable cells was determined by an MTS assay [one-step 3-(4,5-dimethylthiazol-2-yl)-2,5-diphenyltetrazolium bromide assay; Promega Corporation, Madison, WI]. Cellular triglyceride (TG) and cholesterol (TCHO) contents were measured with TG Test Wako and Cholesterol Test Wako kits (Wako, Osaka, Japan) according to the manufacturer's instructions.

Equilibrium ultracentrifugation of JFH-1 particles in isopycnic iodixanol gradients. Filtered supernatant fluids collected from JFH-1 RNA- and pre-miRNA- or anti-miRNA-transfected cell cultures were concentrated 30-fold with a Centricon PBHK Centrifugal Plus-20 filter unit with an Ultracel PL membrane (100-kDa exclusion; Merck Millipore, Billerica, MA) and then layered on top of a preformed continuous 10 to 40% iodixanol (OptiPrep; Sigma-Aldrich) gradient in Hanks' balanced salt solution (Invitrogen, Carlsbad, CA) as described previously (24). The gradients were centrifuged in an SW41 rotor (Beckman Coulter Inc., Brea, CA) at 35,000 rpm for 16 h at 4°C, and the fractions (500 μl each) were collected from the top of the tube. The density of each fraction was determined with a digital refractometer (Atago, Tokyo, Japan).

Infectivity assays. Huh-7.5 cells were seeded at 5.0×10^4/well in 48-well plates 24 h before inoculation with 100 μl of the gradient fractions. The cells were tested for the presence of intracellular core antigen by immunofluorescence 72 h later, as described below. Clusters of infected cells that stained for the core antigen were considered to constitute a single infectious focus, and virus titers were calculated accordingly in terms of numbers of focus-forming units (FFU)/ml.

Western blotting and immunofluorescence staining. Western blotting was performed as described previously (27). The cells were washed in PBS and lysed in radioimmunoprecipitation assay buffer containing Complete protease inhibitor cocktail and PhosSTOP (Roche Applied Science, Indianapolis, IN). The membranes were blocked in Blocking One or Blocking One-P solution (Nacalai Tesque, Kyoto, Japan), and the expression of HCV core protein, retinoid X receptor alpha (RXRα), sterol regulatory element-binding protein (SREBP1), ATP-binding cassette subfamily A member 1 (ABCA1), ApoE3, ApoB100, fatty acid synthase (FASN), peroxisome proliferator-activated receptor α (PPARα), ApoA1, phospho-PKR-like ER kinase (phospho-PERK), PERK, phospho-eIF2α, eIF2α, BIP, phospho-STAT1, and β-actin was evaluated with mouse anti-core (Thermo Fisher Scientific Inc., Rockford, IL), rabbit anti-RXRα, rabbit anti-SREBP1 (Santa Cruz Biotechnology Inc., Santa Cruz, CA), mouse anti-ABCA1 (Abcam, Cambridge, MA), goat anti-ApoE3, goat anti-ApoB100 (R&D Systems Inc., Minneapolis, MN), rabbit anti-FASN, rabbit anti-PPARα, mouse anti-ApoA1, rabbit anti-phospho-PERK, rabbit anti-PERK, rabbit anti-phospho-eIF2α, rabbit anti-eIF2α, rabbit anti-BIP, rabbit anti-phospho-STAT1, and rabbit anti-β-actin antibodies (Cell Signaling Technology Inc., Danvers, MA), respectively.

For immunofluorescence staining, the cells were washed twice with PBS and fixed in 4% paraformaldehyde for 15 min at room temperature. After washing again with PBS, the cells were permeabilized with 0.05% Triton X-100 in PBS for 15 min at room temperature. They were then incubated in a blocking solution (10% FBS and 5% BSA in PBS) for 30 min and with the anti-core monoclonal antibodies. The fluorescent secondary antibodies were Alexa 568-conjugated anti-mouse IgG antibodies (Invitrogen). Nuclei were labeled with 4′,6-diamidino-2-phenylindole (DAPI), and LDs were visualized with boron-dipyrromethene (BODIPY) 493/503 (Invitrogen). Imaging was performed with a CSU-X1 confocal microscope (Yokogawa Electric Corporation, Tokyo, Japan).

Quantitative RTD-PCR. Total RNA was isolated with a GenElute Mammalian Total RNA Miniprep kit (Sigma-Aldrich), and cDNA was synthesized with a high-capacity cDNA reverse transcription kit (Applied Biosystems, Carlsbad, CA). The primer pairs and probes for C/EBPα, ABCA1, PPARγ, SREBF1, SREBF2, FASN, 2′-5′-oligoadenylate synthetase 2 (OAS2), and β-actin were obtained from the TaqMan assay reagent library. HCV RNA was detected as described previously (28). HCV RNA was isolated from viral particles with a QIAamp viral RNA kit (Qiagen, Inc., Valencia, CA) in accordance with the manufacturer's instructions. Total RNA containing miRNA was isolated according to the protocol of the mirVana miRNA isolation kit (Ambion). For the enrichment of mature miRNA, argonaute 2 (Ago2)-binding miRNA was immunoprecipitated with an anti-Ago2 monoclonal antibody (Wako) and mature miRNA was eluted from the precipitant with a microRNA isolation kit, Human Ago2 (Wako). cDNA was prepared via reverse transcription with 10 ng of isolated total RNA and 3 μl of each reverse transcription primer with specific loop structures. Reverse transcription was performed with a TaqMan MicroRNA reverse transcription kit (Applied Biosystems) according to the manufacturer's protocol. RTD-PCR was performed with the 7500 Real Time PCR system (Applied Biosystems) according to the manufacturer's instructions. The primer pairs and probes for miR-let7a, miR-34c, miR-142-5p, miR-27a, miR-23a, and RNU6B were obtained from the TaqMan assay reagent library.

3′ UTR luciferase reporter assays. The miRNA expression reporter vector pmirGLO Dual-Luciferase miRNA Target Expression Vector (Promega Corporation) was used to validate the RXRα and ABCA1 3′ untranslated regions (UTRs) as miRNA binding sites. cDNA fragments corresponding to the entire 3′ UTR of human RXRα and human ABCA1 were amplified with the Access RT-PCR system (Promega Corporation) from total RNA extracted from Huh-7.5 cells. The PCR products were cloned into the designated multiple cloning site downstream of the luciferase open reading frame between the SacI and XhoI restriction sites of the pCR2.1-TOPO vector (Invitrogen). Point mutations in the seed region of the predicted miR-27a sites within the 3′ UTR of human RXRα and human ABCA1 were generated with a QuikChange Multi site-directed mutagenesis kit (Agilent Technologies Inc., Santa Clara, CA) according to the manufacturer's protocol. All constructs were confirmed by sequencing.

Huh-7.5 cells were grown to 70% confluence in 24-well plates in complete DMEM. The cells were cotransfected with 200 ng of the indicated 3′ UTR luciferase reporter vector and 50 nM synthetic miRNA (pre-miRNA) or 50 nM anti-miRNA (Ambion) in a final volume of 0.5 ml with Lipofectamine 2000 (Invitrogen). At 24 h posttransfection, firefly and *Renilla* luciferase activities were measured consecutively with the Dual-Luciferase Reporter Assay system (Promega Corporation).

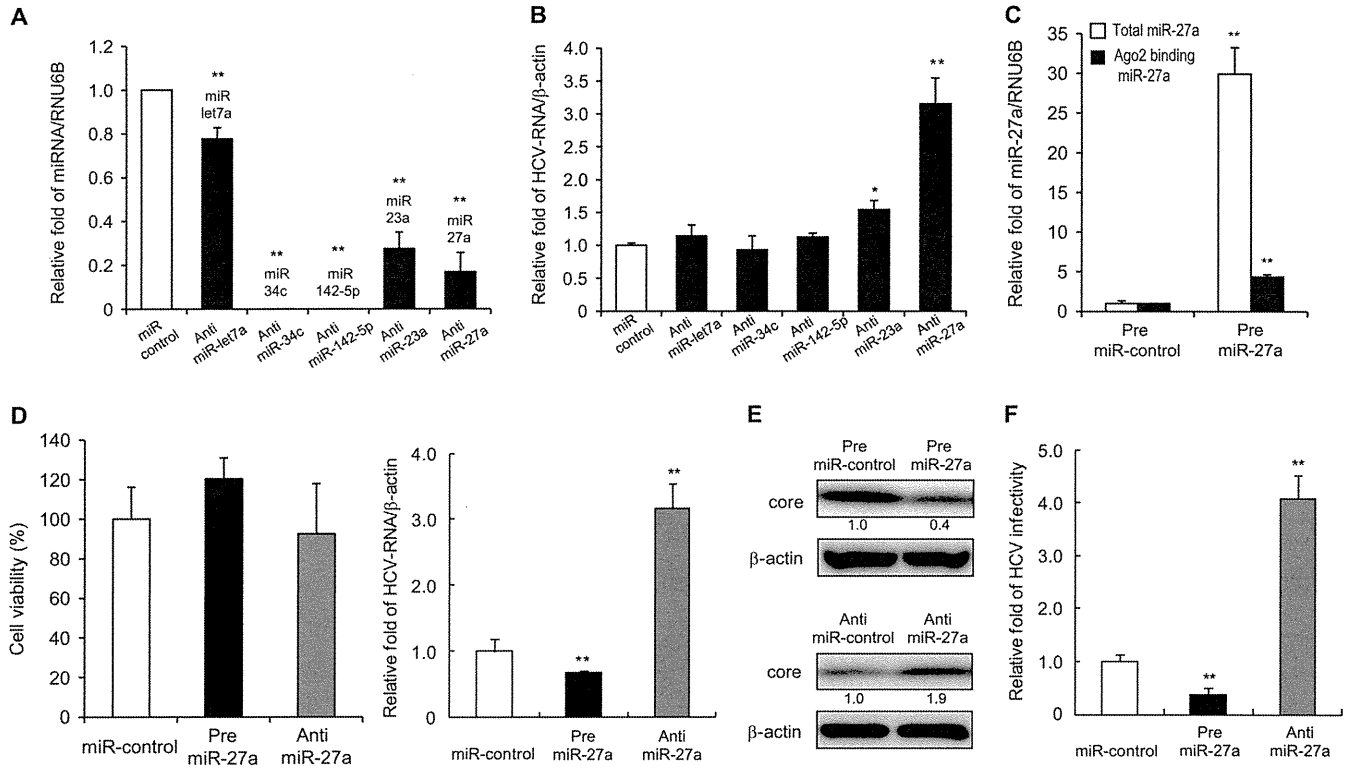

FIG 1 miR-27a has a negative effect on HCV replication and infectivity. Huh-7.5 cells were transfected with JFH-1 RNA and pre- or anti-miRNA. Expression was quantified at 72 h posttransfection. (A) Inhibition efficiency of miRNAs by anti-miRNAs (RTD-PCR, $n = 6$). (B) Effects of anti-miRNAs on HCV replication (RTD-PCR, $n = 6$). (C) Detection of whole miR-27a and Ago2-binding miR-27a in Huh-7.5 cells. At 72 h posttransfection, cells were harvested and Ago2-binding miRNA was purified as described in Materials and Methods. White bars indicate total miR-27a levels, and black bars indicate Ago2-binding miR-27a levels (RTD-PCR, $n = 6$). (D) Effects of pre- or anti-miR-27a on cell viability (left) and HCV replication (right). Cell viability (%) was assessed by the MTS assay ($n = 6$). (E) Effects of pre- or anti-miR-27a on HCV core protein levels by Western blotting. (F) Effects of pre- or anti-miR-27a on HCV infection. Huh-7.5 cells were infected with HCVcc derived from Huh-7.5 cells transfected with pre- or anti-miR-27a and JFH-1 RNA. HCV RNA was quantified at 72 h postinfection by RTD-PCR ($n = 6$). All experiments were performed in duplicate and repeated three times. Values are means ± standard errors. *, $P < 0.01$; **, $P < 0.005$.

Promoter analysis. DNA fragments from −400 to +36 bp and from −700 to +36 bp relative to the transcription initiation site of pri-miR-23a~27a~24-2 were inserted into pGL3-Basic (Promega Corporation) at the MluI and XhoI sites. Point mutations in the seed region of predicted C/EBPα binding sites were generated with a QuikChange Multi site-directed mutagenesis kit (Agilent Technologies) according to the manufacturer's protocol. All constructs were confirmed by sequencing.

Huh-7.5 cells transfected with HCV RNA were cultured for 24 h in 24-well plates, and then 200 ng of the plasmids was cotransfected with 2 ng of the *Renilla* luciferase expression vector (pSV40-Renilla) with the FuGENE6 Transfection Reagent (Roche Applied Science). After 24 h, the cells were treated with oleic acid in the presence of 2% FFA-free BSA (Sigma-Aldrich). At 48 h posttreatment, a luciferase assay was carried out with the Dual-Luciferase Reporter Assay system (Promega Corporation) according to the manufacturer's instructions.

For tunicamycin treatment, the plasmids (200 ng) were cotransfected with 2 ng pSV40-Renilla with FuGENE6 (Roche Applied Science) into Huh-7.5 cells grown in the wells of 24-well plates. After 24 h, the cells were treated for a further 24 h with the indicated concentrations of tunicamycin and a luciferase assay was carried out as described above.

RNA interference. A small interfering RNA (siRNA) specific to ABCA1 and a control siRNA were obtained from Thermo Fisher Scientific. Transfection was performed with Lipofectamine 2000 (Invitrogen) according to the manufacturer's instructions.

IFN treatment. Huh-7.5 cells transfected with HCV RNA and pre- or anti-miRNA were treated with oleic acid as described above. At 48 h later, the cells were treated with the indicated number of international units of IFN-α for 24 h.

Affymetrix GeneChip analysis. Aliquots of total RNA (50 ng) isolated from the cells were subjected to amplification with the WT-Ovation Pico RNA Amplification system (NuGen, San Carlos, CA) according to the manufacturer's instructions. The Affymetrix Human U133 Plus 2.0 microarray chip containing 54,675 probes has been described previously (29).

Statistical analysis. Results are expressed as mean values ± standard errors. At least six samples were tested in each assay. Significance was tested by one-way analysis of variance with Bonferroni methods, and differences were considered statistically significant at P values of <0.01 (*, $P < 0.01$; **, $P < 0.005$).

Microarray accession number. The expression data determined in this study were deposited in the Gene Expression Omnibus database (NCBI) under accession number GSE41737.

RESULTS

Functional relevance of the upregulated miRNAs in HCV-infected livers. Previously, 19 miRNAs were shown to be differentially expressed in HBV- and HCV-infected livers (2). Of these, 6 miRNAs were upregulated and 13 were downregulated. In this study, we focused on the upregulated miRNAs, as they might play a positive role in HCV replication. Anti-miRNAs and the control miRNA were transfected into Huh-7.5 cells following JFH-1 RNA